

Algorithm for Optimized mRNA Design Improves Stability and Immunogenicity

He Zhang,^{1,2†} Liang Zhang,^{1,2†} Ang Lin,^{3†} Congcong Xu,³ Ziyu Li,¹
Kaibo Liu,^{1,2} Boxiang Liu,¹ Xiaopin Ma,³ Fanfan Zhao,³ Weiguo Yao,³
Hangwen Li,³ David H. Mathews,^{4,5,6} Yujian Zhang,^{3*} Liang Huang^{1,2,†,*,◊}

¹Baidu Research USA, Sunnyvale, CA 94089, USA

²School of EECS, Oregon State University, Corvallis, OR 97330, USA

³Stemirna Therapeutics Inc., Shanghai 201206, China

⁴Dept. of Biochemistry & Biophysics, ⁵Center for RNA Biology, and

⁶Dept. of Biostatistics & Computational Biology,

University of Rochester Medical Center, Rochester, NY 14642, USA

[†]Equal contribution. ^{*}To whom correspondence should be addressed ([◊]Lead contact).

E-mail: liang.huang.sh@gmail.com; zhangyujian@stemirna.com.

Messenger RNA (mRNA) vaccines are being used for COVID-19 (1, 2, 3), but still suffer from the critical issue of mRNA instability and degradation, which is a major obstacle in the storage, distribution, and efficacy of the vaccine (4). Previous work showed that optimizing secondary structure stability lengthens mRNA half-life, which, together with optimal codons, increases protein expression (5). Therefore, a principled mRNA design algorithm must optimize *both* structural stability and codon usage to improve mRNA efficiency. However, due to synonymous codons, the mRNA design space is prohibitively large, e.g., there are $\sim 10^{632}$ mRNAs for the SARS-CoV-2 Spike protein, which poses insurmountable challenges to previous methods. Here we provide a surprisingly simple solution to this hard problem by reducing it to a classical problem in computational linguistics, where finding the optimal mRNA is akin to finding the most likely sentence among similar sounding alternatives (6). Our algorithm, named *LinearDesign*, takes only 11 minutes for the Spike protein, and can jointly optimize stability and codon usage. Experimentally, without chemical modification, our

designs substantially improve mRNA half-life and protein expression *in vitro*, and dramatically increase antibody response by up to 23× *in vivo*, compared to the codon-optimized benchmark. Our work enables the exploration of highly stable and efficient designs that are previously unreachable and is a timely tool not only for vaccines but also for mRNA medicine encoding all therapeutic proteins (e.g., monoclonal antibodies and anti-cancer drugs (7, 8)).

Messenger RNA (mRNA) vaccines (9, 10) emerged as a promising tool against COVID-19 thanks to their scalable production, safety, and efficacy (1, 2, 3). However, among other limitations, they still suffer from the critical issue of chemical instability and degradation of the largely single-stranded and fragile mRNA molecule both in solution and *in vivo*. This instability has become a major obstacle in the storage and distribution of the vaccine, requiring the use of cold-chain technologies that hinders its use in developing countries (4). More importantly, the *in vivo* instability of mRNAs leads to insufficient protein expression (5), and in turn, compromised immunogenicity. While chemical stability is hard to model, previous work established its correlation with secondary structures, as quantified by the well-studied thermodynamic folding stability. This structural stability, along with optimal codon usage, leads to greater protein expression (5). Therefore, a principled mRNA design algorithm needs to optimize *both* structural stability and codon usage to enhance mRNA translation efficiency.

However, this mRNA design problem is extremely challenging due to the exponentially large search space.¹ Each amino acid is encoded by a triplet codon, i.e., three adjacent nucleotides, but due to redundancies in the genetic code ($4^3 = 64$ codons for 20 amino acids), most amino acids have multiple codons. This combinatorial explosion results in a prohibitively large number of candidates. For example, the Spike protein of SARS-CoV-2 with 1,273 amino acids can be encoded by $\sim 2.4 \times 10^{632}$ mRNA sequences (Fig. 1A). This poses an insurmountable computational challenge to jointly optimize structural stability and codon usage, and rules out enumeration which takes $\sim 10^{616}$ billion years for the Spike protein (Fig. 1B). On the other hand, the conventional approach to mRNA design, *codon optimization* (12), only optimizes codon usage but barely improves stability, leaving out

¹Our work only designs the coding region, and is independent of the untranslated regions (UTRs).

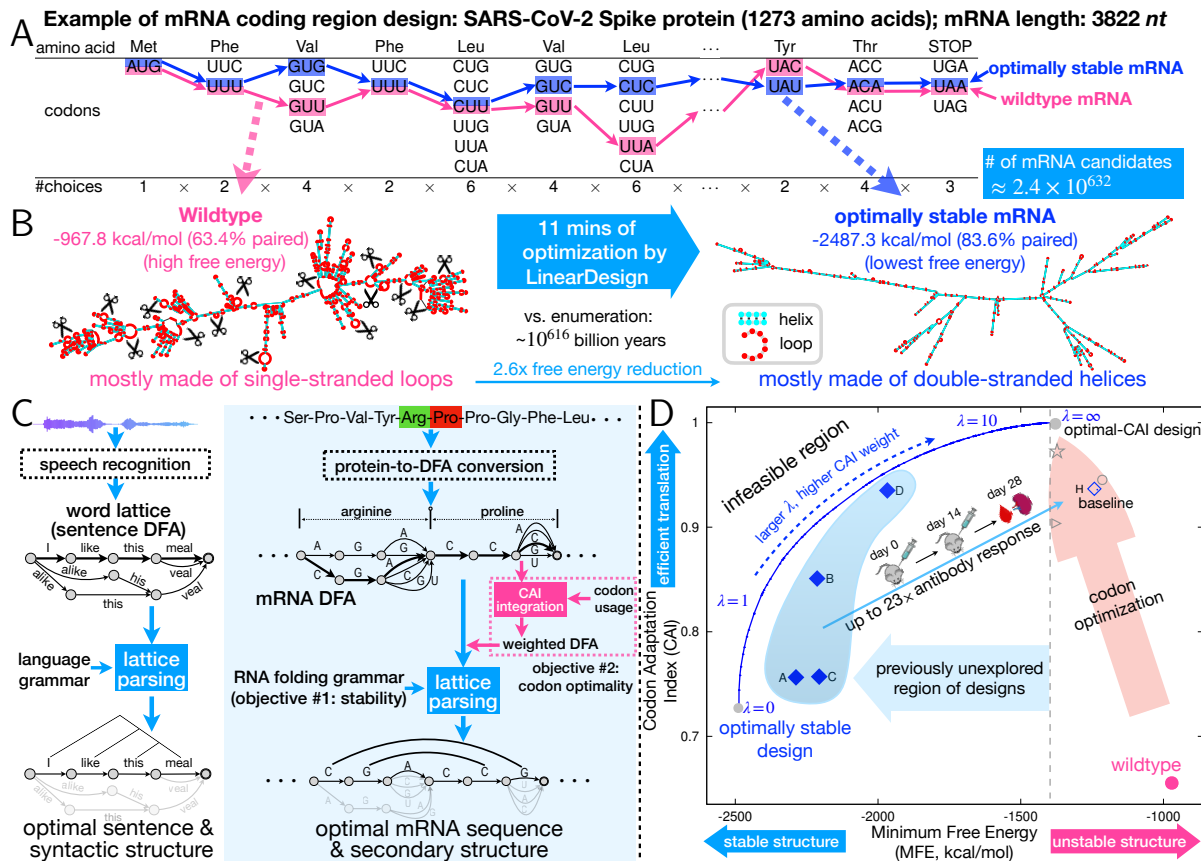


Figure 1: Overview of mRNA coding region design for two well-established objectives, *stability* and *codon optimality*, using SARS-CoV-2 Spike protein as an example. **A**: Due to combinatorial explosion, there are $\sim 10^{632}$ mRNAs for the Spike protein. The pink and blue paths represent the wildtype and the optimally stable (i.e., lowest energy) design found by our work, respectively. **B**: There are vastly different secondary structures between these two sequences, with the former being mostly single-stranded (thus prone to degradation \gg) and the latter being mostly double-stranded. Our algorithm LinearDesign takes just 11 minutes for this optimization while enumeration needs $\sim 10^{616}$ billion years. **C**: We borrow deterministic finite-state automaton (DFA) and lattice parsing from language (left) for mRNA design (right). An mRNA DFA, inspired by “word lattice”, compactly represents all mRNA candidates. Lattice parsing folds all sequences in this DFA with an RNA folding grammar to find the optimally stable mRNA (Fig. 2B), and can also incorporate codon optimality using a weighted DFA (Fig. 2D). **D**: Visualization of the mRNA design space for the Spike protein, with stability on the x -axis and codon optimality on the y -axis. The conventional mRNA design method, used by the COVID-19 vaccines of BioNTech-Pfizer (\circ), Moderna (\star), and CureVac (\triangleright), is *codon optimization* (11), which improves codon usage (the \uparrow arrow), but leaves out the high-stability region (left of the dashed line). LinearDesign, by contrast, jointly optimizes stability and codon optimality (the blue curve, with λ being the weight of the latter). By considering other factors, we select a few of our designs (four shown here: \blacklozenge A–D) for experiments (Fig. 4), which show up to 23 \times antibody responses over the codon-optimized baseline ($H\blacklozenge$).

the huge space of highly stable mRNAs (Fig. 1D). Optimizing the other widely considered factor, GC-content, has a similar effect as it correlates with codon usage in vertebrates (13). As a result, the vast majority of highly stable designs remains unexplored.

Here we provide a surprisingly simple algorithm, *LinearDesign*, to solve this challenging problem by reducing it to the classical problem of “lattice parsing” (6) in computational linguistics (Fig. 1C). We show that finding the optimal mRNA among vast space of candidates is analogous to finding the most grammatical sentence among numerous similar-sounding alternatives. More specifically, we formulate the mRNA design space using a deterministic finite-state automaton (DFA), similar to a “word lattice” (6), which compactly encodes exponentially many mRNA candidates (Figs. 1–2). We then use lattice parsing to find the most stable mRNA in the DFA without enumeration (Fig. 2B), which can also jointly optimize stability and codon optimality by representing the latter in a *weighted* DFA (Fig. 2D). This unexpected connection to natural language enables an efficient algorithm that scales *quadratically* with the mRNA sequence length in practice, taking only 11 minutes to design the most stable mRNA encoding the SARS-CoV-2 Spike protein. This optimal design has a mostly double-stranded secondary structure vastly different from the largely single-stranded wildtype, thus being much more stable than the latter (Fig. 1B). In this sense, our work turns the enormous search space into a *blessing* (freedom of design) rather than an obstacle. We also develop an even faster (linear-time) variant (Fig. 3A) that provides suboptimal designs for vaccine development. More importantly, experimental results confirmed that, compared to the codon-optimized benchmark, our designs substantially improve chemical stability *in vitro*, protein expression *in cell*, and immunogenicity *in vivo* (Figs. 1& 4). In particular, our designed molecules increase antibody response by up to 23× in mice. Our work provides a timely and promising tool not only for mRNA vaccines, but also for mRNA medicine which has shown great potential to revolutionize healthcare (14), as *LinearDesign* can optimize mRNAs encoding all therapeutic proteins including monoclonal antibodies (7) and anti-cancer drugs (8).

Formulations and Algorithms

Previous work (5) established two main objectives for mRNA design, stability and codon optimality, which synergize to increase protein expression. To optimize for stability, given a protein sequence, we aim to find the mRNA sequence that has the *lowest minimum folding free energy change* (MFE) among all possible mRNA sequences encoding that protein (Fig. S2A), which is a *minimization within a minimization*. Naively, for each candidate

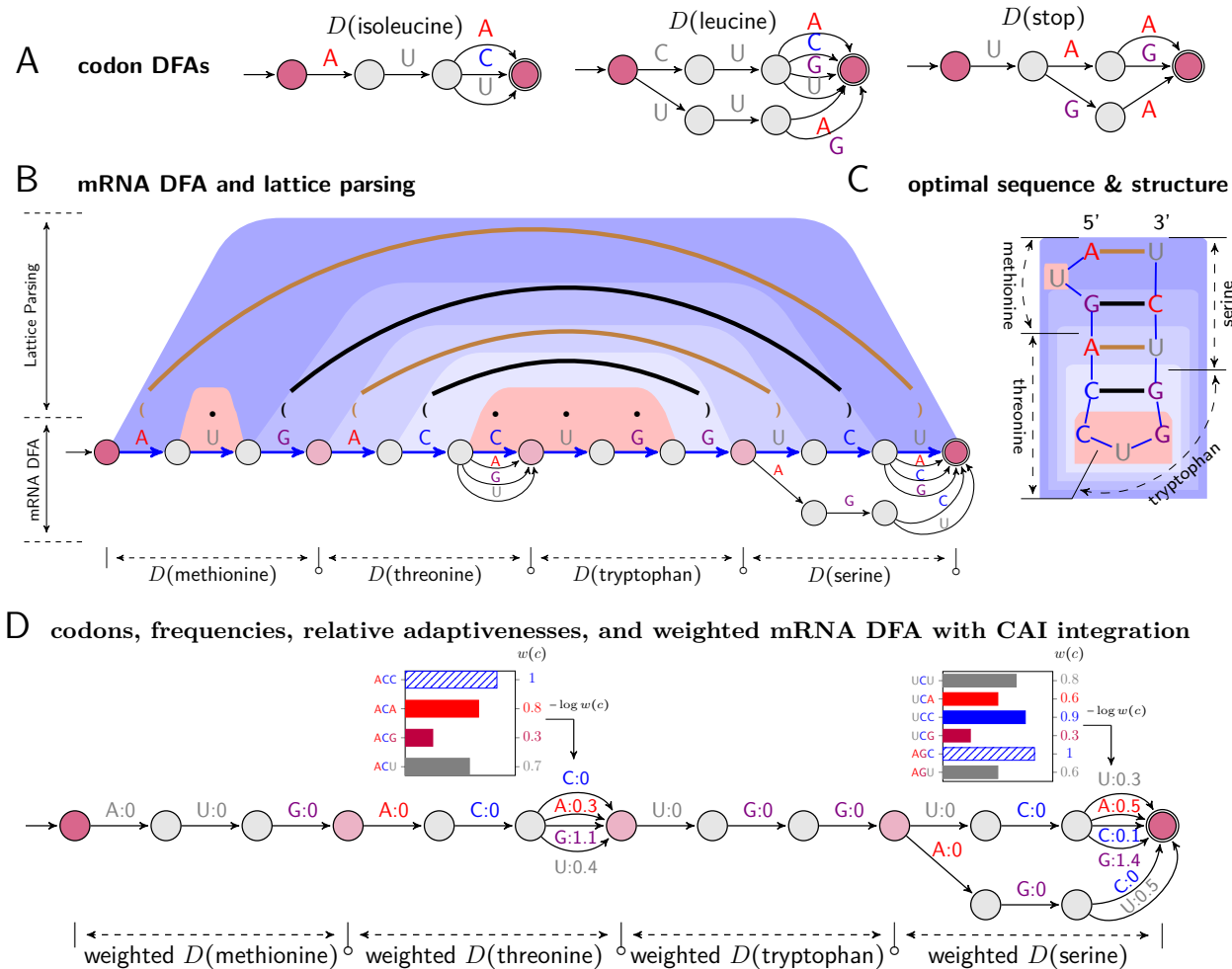


Figure 2: Lattice parsing solves the mRNA design problem, either optimizing stability alone (objective 1; see **A–C**) or jointly optimizing both stability and codon optimality (objectives 1 & 2; see **D**). **A**: Codon DFAs. **B**: An mRNA DFA (bottom) and lattice parsing on that DFA (top). In the DFA, the optimal mRNA sequence under the simplified energy model (Fig. S2E) is shown in the thick blue path, together with its optimal structure shown in the dot-bracket format (“•”: unpaired; “(” and “)””: base pairs). In lattice parsing, the brown and black arcs also depict base pairs (two GC pairs and two AU pairs), while the round trapezoid shadings depict the decomposition of the optimal structure. Among all mRNA sequences encoded in the DFA, lattice parsing finds the optimal sequence with its optimal structure, achieving the lowest free energy under this energy model (where GC and AU pairs have -3 and -2 kcal/mol, respectively). **C**: Another illustration of the optimal sequence and secondary structure in **B**. Next, we show in **D** how to do the joint optimization by integrating codon optimality in weighted DFAs. **D**: Top: bar charts showing the codon frequencies of threonine and serine. The relative adaptiveness $w(c)$ of a codon c is the ratio between the frequencies of c and its most frequent codon (shown in stripes). Bottom: a weighted mRNA DFA encodes each candidate’s CAI in the total weight of its corresponding path, by taking $-\log w(c)$ as edge weights to represent the cost of choosing codon c (see Methods §1.1). This weighted DFA can be plugged back into lattice parsing for joint optimization between stability and codon optimality.

mRNA sequence, we find its MFE structure among all of its possible secondary structures, and then choose the sequence with the lowest MFE. But that would take billions of years, so we need an efficient algorithm that solves the problem without enumeration.

Next, we also aim to jointly optimize mRNA stability and codon optimality (Fig. S2B). The latter is often measured by the Codon Adaptation Index (CAI) (15) defined as the geometric mean of the relative adaptiveness of each codon in the mRNA. Because CAI is between 0 and 1 but MFE is generally proportional to the sequence length, we multiply the logarithm of CAI by the number of codons in the mRNA, and use a hyperparameter λ to balance MFE and CAI ($\lambda = 0$ being MFE-only). See Methods §1.1 for details.

We next describe our solution to these two optimization problems with two ideas borrowed from natural language: DFA (lattice) representation and lattice parsing.

Design Space Representation: DFA (Lattice) Inspired by the “word lattice” representation of ambiguities in computational linguistics, we represent the choice of codons for each amino acid using a similar lattice, or more formally, a DFA, which is basically a directed graph with labeled edges (Figs. 2A & S2C; see Methods §1.2 for formal definitions). After building a codon DFA for each amino acid, we then concatenate them into a single *mRNA DFA*, where each path from the start state to the final state represents a possible mRNA sequence that encodes that protein (see Figs. 2B & S2D).

Objective 1 (Stability): Lattice Parsing RNA folding is well-known to be equivalent to natural language parsing, with a stochastic context-free grammar (SCFG) representing the folding energy model (16) (see Fig. S2E–F). But for mRNA design, the big question is, how to fold all the mRNA sequences in the DFA together? We borrow the idea of “lattice parsing” (17, 6), which generalizes single-sequence parsing to handle all sentences in the lattice simultaneously to find the most likely one (Figs. 1C & S1). Similarly, we use lattice parsing to fold all sequences in the mRNA DFA simultaneously to find the most stable one (Figs. 2B & S2G–H). Note that single-sequence folding is a special case with a single-chain DFA. This process can also be interpreted as SCFG-DFA intersection (Fig. S2A) where the SCFG scores for stability and the DFA demarcates the set of candidates. This algorithm runs in the same worst-case $O(n^3)$ time as single-sequence folding (but with a larger constant) where n is the mRNA length (Methods §1.3), but for practical applications it

only scales $O(n^2)$ (Fig. 3A).

Adding Objective 2 (Codon Optimality): Lattice Parsing with Weighted DFAs

We now extend DFAs to *weighted DFAs* (WDFAs) to integrate codon optimality on edge weights. Since our joint optimization formulation factors CAI onto the relative adaptiveness $w(c)$ of each individual codon c , we set edge weights in each codon DFA so that a codon c has path cost $-\log w(c)$. Then in a weighted mRNA DFA, the cost of each start-end path is the sum of $-\log w(c)$ for each codon c in the corresponding mRNA, which is proportional to its $-\log$ CAI (Fig. 2D). Now lattice parsing takes a stochastic grammar (for stability) and a weighted DFA (for codon optimality) and solves the joint optimization, which can be viewed as the weighted intersection between SCFG and WDFA (Fig. S2B; Methods §1.4). By contrast, two previous efforts at stabilizing mRNAs (18, 19) using ad-hoc algorithms can not jointly optimize codon usage; see Methods §1.8 for details.

Expressiveness of DFAs Our DFA framework can also represent alternative genetic codes, modified nucleotides, and coding constraints; see Figs. S6–S7 and Methods §1.7.

Linear-time Approximation The exact design algorithm might still be slow for long sequences. On the other hand, suboptimal designs may also be worth exploring for wet lab experiments (see below), due to the many other factors involved in mRNA design besides stability and codon usage. So we developed an approximate search version that runs in linear time using beam search, keeping only the top b most promising items per step (b is the beam size), inspired by our previous work LinearFold (20).

***In silico* Results and Analysis**

Fig. 3A benchmarked the runtime of LinearDesign on UniProt proteins (21). LinearDesign was shown in a combination of two optimization objectives, MFE-only (objective 1) vs. MFE+CAI (objectives 1 & 2), and two search modes, exact search vs. beam search (beam size $b = 500$). Empirically, LinearDesign scales quadratically with mRNA sequence length n for practical applications ($n < 10,000$ nt) thanks to the DFA representation and lattice parsing (see Fig. S8 for analysis). Next, our CAI-integrated exact search (CAI weight $\lambda = 4$) had the same empirical complexity, and was only $\sim 15\%$ slower than the

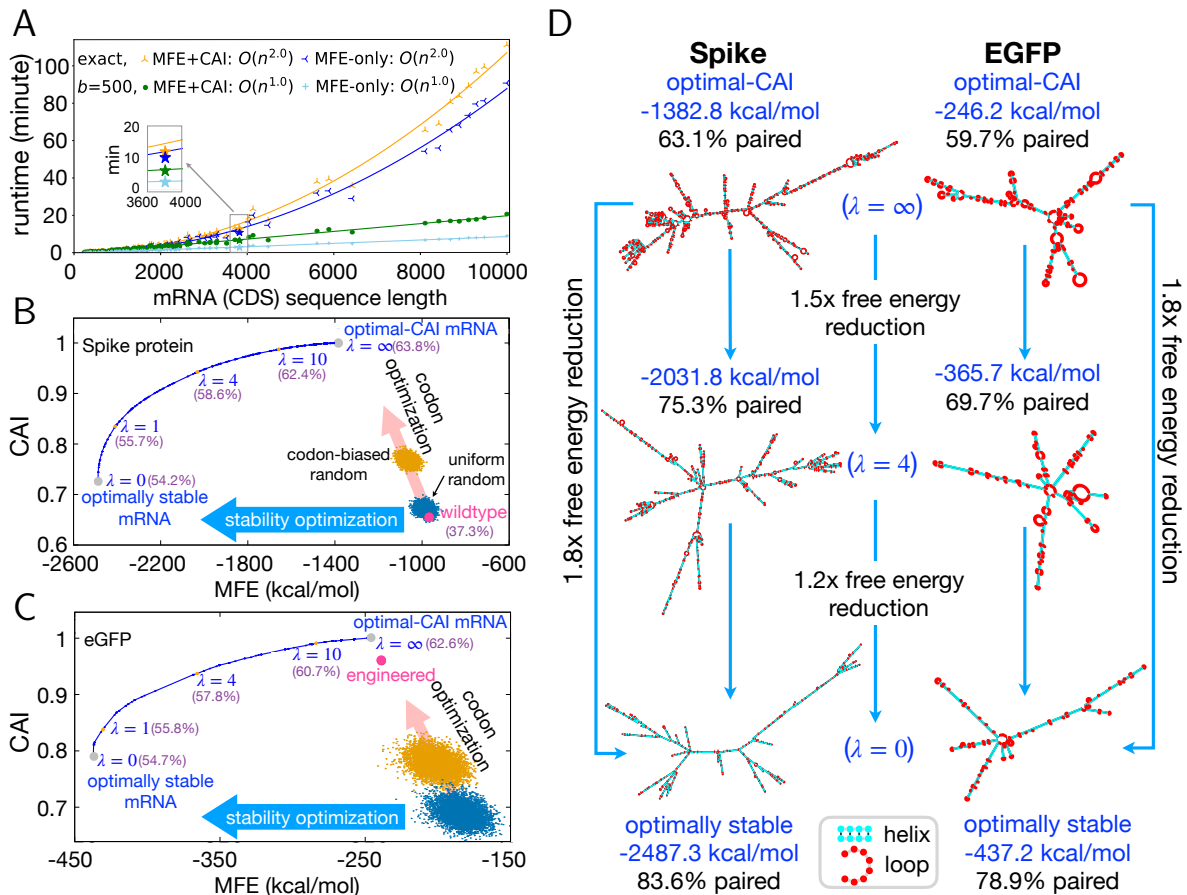


Figure 3: *In silico* analysis of LinearDesign. **A**: Runtime visualization of LinearDesign on UniProt proteins. Overall, our exact search only scales quadratically with sequence length in practice (see Fig S8 for analysis), and our MFE+CAI mode (with $\lambda = 4$) is only $\sim 15\%$ slower than our MFE-only version. Moreover, beam search ($b = 500$) significantly speeds up long sequences, with minor search errors (see also Fig. S9). **B–C**: 2D (MFE–CAI) visualizations of Spike protein (**B**) and eGFP (**C**) designs, respectively (both using human codon preference). The blue curves (varying λ from 0 to ∞) achieve the best MFE for a given CAI, and vice versa, thus forming the feasibility limit. GC% are shown in parentheses for LinearDesign-generated sequences. The human genome prefers GC-rich codons, therefore codon optimization (the pink arrows in **B–C**) also improves stability, but only marginally, as the two optimization directions (codon vs. stability) are largely orthogonal. By contrast, Fig. S10B shows that with an AU-rich codon preference, codon optimization decreases stability. **D**: Secondary structures of example designs. The optimal-CAI designs (top, $\lambda = \infty$) are largely single-stranded ($\sim 60\%$ paired), while the optimally stable designs (bottom, $\lambda = 0$) are mostly double-stranded ($\sim 80\%$ paired). We also show intermediate designs (e.g., $\lambda = 4$) that compromise between stability and CAI. See also Fig. S10A–B for the case of negative λ 's.

MFE-only version thanks to the convenience of adding CAI in our DFA representation. Last, our beam search version ($b = 500$) further speeds up our design and scales *linearly* with sequence length, taking only 2.7 minutes (vs. 10.7 minutes for exact search) on the SARS-CoV-2 Spike protein (for MFE-only), with an approximation error (i.e., energy gap

%, defined as $1 - \text{MFE}_{\text{approx_design}}/\text{MFE}_{\text{exact_design}}$) of just 1.2%. In fact, as sequences get longer, this percentage stabilizes, suggesting that beam search quality does not degrade with sequence length; see Fig. S9 for details.

As shown in Figs. 3B–C, for a GC-favoring codon preference (such as human), the conventional codon optimization method does improve stability, but only slightly, since its optimization directions (the pink arrows) are largely orthogonal to the stability optimization directions (the blue arrows). By contrast, our LinearDesign can directly optimize stability and find the optimally stable mRNAs ($\lambda = 0$) on both the Spike protein and the enhanced gene fluorescent protein (eGFP), which have the lowest MFEs that are 1.8 \times lower than the optimal-CAI’s ($\lambda = \infty$). Also, our optimally stable designs have mostly double-stranded secondary structures (Fig. 3D), which are predicted to be much less prone to degradation (5). LinearDesign also finds the sequence with the lowest MFE for a given CAI and vice versa, thus forming the feasibility limit of mRNA design (the blue curves in Fig. 3B–C, with λ ranging from 0 to ∞). Furthermore, when the codon bias prefers AU-rich codons (such as yeast), codon optimization actually *worsens* stability (Fig. S10).

***In vitro* and *In vivo* Experimental Results**

We performed experimental assays to study the chemical stability, protein expression, and immunogenicity of LinearDesign-generated mRNA molecules (Fig. 4). All mRNA sequences in this study encode the SARS-CoV-2 Spike protein without the 2P mutation (22), with unmodified (natural) nucleotides and the same UTRs. We used LinearDesign (with beam search plus a k -best algorithm (23) for suboptimal candidates) to generate seven mRNA sequences ($\blacklozenge_{\text{A-G}}$ in Fig. 4A), which were compared to the benchmark sequence (baseline $\text{H}\blacklozenge$) designed by a commonly-used codon optimization algorithm, OptimumGeneTM. The seven LinearDesign sequences were selected to be widely distributed in the unexplored high-stability territory (the region in Fig. 4A where $\text{MFE} < -1,400$ kcal/mol, inaccessible to codon optimization), and to separate the impacts of MFE and CAI, we designed sequences that are almost identical in either MFE (B–C // D–E–F) or CAI (A–C–F // B–E // D–G–H). It is well-known that translation efficiency drops if the 5'-leader region is particularly structured (5), so we did not optimize for the first 5 amino acids and used a heuristic to select the first 15 nucleotides. It is also suggested that long

stems may induce unwanted innate immune responses (24), so we avoided them in our designs, which is why we did not study the lowest-MFE candidates closest to the optimal boundary (the blue curve) which usually contain long stems. See Methods §1.10 for details. It is worth mentioning that some UTR structures are crucial for translation (25), and we observe that our stable designs (A–F), having more structured coding regions, form fewer base pairs with, and thus interfere less with the structures of, commonly used UTRs than codon-optimized ones (Tab. S2). This suggests that LinearDesign is likely to be effective independent of the choice of UTRs.

In-solution Structure Compactness and Chemical Stability We then studied the structure compactness of mRNA molecules, which is hypothesized to be correlated with the folding free energy change. We performed Electrophoretic Mobility Shift Assay (EMSA) using Agarose gel electrophoresis at 30°C. An mRNA molecule with a lower MFE contains more secondary structures and thus exhibits more compact shape and smaller hydrodynamic size, which makes it move faster in the agarose gel matrix. We can see that the gel mobility pattern in Fig. 4B correlated with the MFEs of the eight designs almost perfectly: sequence A, with the lowest MFE, moved the fastest, followed by sequences B and C, then by sequences D, E, and F, then by sequence G, and finally by the baseline sequence H, which has the highest MFE.

To evaluate the chemical stability, we incubated the designed mRNA molecules in RNA storage buffer (Thermo Fisher) at 37°C followed by quantification of intact mRNA as a function of time. Overall, the chemical stability results also correlated well with the MFEs. The lowest-MFE design (A) degraded the slowest, and the highest-MFE baseline (H) the fastest, followed by the design (G) with the second highest MFE. For example, after day 4, there was only 2.8% intact molecules of H and 18.1% of G, while design A still had 36.9% and four other designs (B–D and F) also had around 30%. After day 5, sequence H had 0% remaining, sequence G had 8.8%, but the lower-MFE designs (A–F) still had 14.7%–19.2% left (Fig. 4C). These results suggest that low-MFE designs have longer half-lives, which will contribute to higher protein expression levels (see below).

Cellular Protein Expression Sufficient antigen expression is one of the prerequisites for the induction of antibody responses so we evaluated the designed mRNA molecules

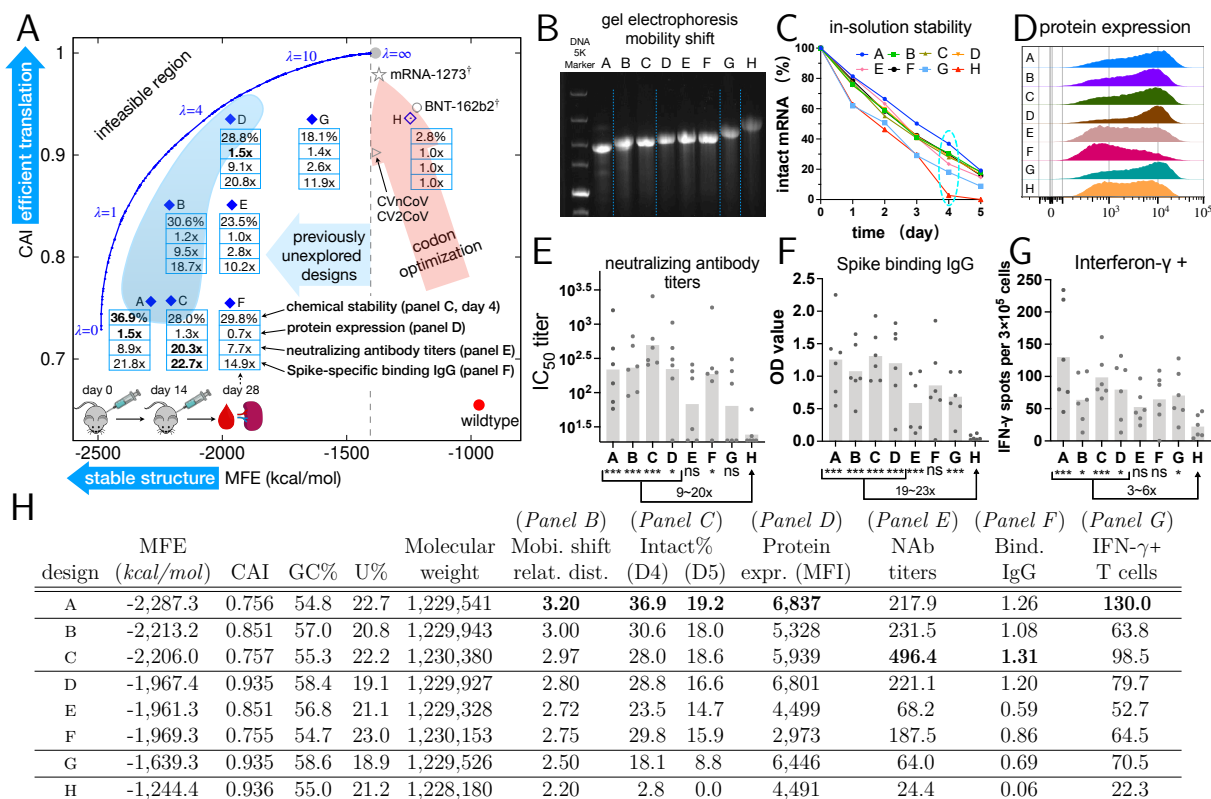


Figure 4: Experimental results of LinearDesign-generated molecules and vaccines for the SARS-CoV-2 Spike protein, using unmodified nucleotides. **A**: Summary of chemical stability (day 4), protein expression, and neutralizing and binding antibody levels for our designs (\blacklozenge A–G) compared to the codon-optimized baseline (H \blacklozenge). **B**: Gel mobility shift using gel electrophoresis correlates perfectly with folding free energy changes. **C**: Chemical stability of mRNAs upon storage in buffer. **D**: Flow cytometric analysis of expression level of Spike protein on cell surface following mRNA transfection into immortalized HEK-293 cells. **E**: Neutralizing antibody titers. **F**: OD values of Spike protein-specific binding IgG. **G**: Frequency of Interferon (IFN)- γ -secreting T cells. We used a two-tailed Mann-Whitney test for significance testing of our designs against the baseline (‘ns’: not significant, ‘*’: $0.01 \leq p < 0.05$, ‘**’: $0.001 \leq p < 0.01$, ‘***’: $p < 0.001$). Overall, our best designs (A–D, in shades) saw substantial improvements in half-life, protein expression, and antibody response (up to 23 \times). **H**: detailed computational and experimental data for the eight designs (MFI: mean fluorescence intensity); see Fig. S11 for their secondary structures. \dagger The vaccines of Moderna and BioNTech use modified nucleotides (26), but their MFEs here are calculated with the standard energy model (27).

for protein expression. The SARS-CoV-2 Spike protein is a transmembrane protein that can be directly detected on viable mRNA-transfected cells by flow cytometry. Following transfection into HEK-293 cells, we measured the amount of Spike proteins generated by all designs after 24 hours. Of note, 5 out of 7 mRNA molecules (designs A–D and G) showed substantially higher protein expression levels than the benchmark H (Fig. 4). For example, designs D and G (with CAIs almost identical to H, but lower MFEs) were 1.5 \times and 1.4 \times better, respectively, and the lowest MFE design A was also 1.5 \times better. In general, our results are consistent with Mauger et al.’s (5) that low MFE and high CAI

synergize to improve protein expression, but we were able to test this hypothesis using mRNA molecules with much lower MFEs than they could, thanks to LinearDesign’s ability to explore the previously unreachable design space.

***In vivo* Immunogenicity** Ultimately, we tested whether our designs could endow mRNA vaccines with higher immunogenicity, which is usually represented by the magnitude of elicited antibody and T cell responses. We employed a lipid based delivery system for LinearDesign-generated mRNA vaccines (28), and further evaluated and compared the immunogenicity of each design side-by-side. C57BL/6 mice were intramuscularly immunized with two doses of vaccines at an interval of 2 weeks. Neutralizing antibodies, Spike protein-specific Immunoglobulin G (IgG), as well as antigen-specific interferon (IFN)- γ -secreting T cells were assessed (see Fig. 4). Interestingly, all vaccine candidates carrying LinearDesign-generated mRNA molecules were able to elicit high levels of binding IgG and neutralizing antibodies. While in contrast, none or low levels of neutralizing antibodies were induced by the benchmark H. Similar results were also observed on the antigen-specific T cell response, where a robust T helper Type 1 (Th1)-biased T cell response was induced only by vaccines containing LinearDesign-generated mRNAs. Overall, our designs A–D, which are closer to the optimal boundary (shaded in Fig. 4A), i.e., strong in both MFE and CAI, led to a surprising 9 ~ 20 \times increase in neutralizing antibody titers and 19 ~ 23 \times increase in OD values for Spike-specific binding antibody than the benchmark (codon-optimized baseline H). These ratios were much higher than the corresponding ratios for cellular protein expression (1.2 ~ 1.5 \times), because the latter was only measured for 24 hours. We suspect that LinearDesign-generated mRNA molecules have longer functional half-lives *in vivo* (beyond 24 hours), which induce higher levels of antibody response.

Discussion

An effective mRNA design strategy is of utmost importance, especially for the development of mRNA vaccines that have shown great promise in fighting the current and future pandemics. However, it is extremely challenging due to the prohibitively large search space. We, instead, presented a surprisingly simple solution to this problem by formulating the design space as DFAs and reducing the mRNA design problem to lattice parsing in computational linguistics. This unexpected cross-disciplinary analogy provides an effi-

cient algorithm that scales $O(n^2)$ for practical applications, taking only 10.7 minutes for the SARS-CoV-2 Spike protein, and can jointly optimize stability and codon optimality using weighted DFAs. Our DFA framework can also apply to non-standard genetic codes, modified nucleotides, and coding constraints such as avoiding certain adjacent codon pairs. Finally, to provide suboptimal candidates for vaccine development and further speed up the design for long sequences, we provide an $O(n)$ -time approximate variant.

The mRNA sequences generated by LinearDesign were comprehensively characterized in this study and demonstrated superiority over the commonly-used codon optimization benchmark in three attributes critical for vaccine performance: chemical stability, translation efficiency, and immunogenicity. In particular, four of our seven designs showed 9~20× increase in neutralizing antibody titers and 19~23× increase in binding antibody levels over the benchmark. Given that chemical modification is widely believed to be critical to the recent success of mRNA vaccines (29, 10, 1, 2),² it is intriguing that our designed mRNAs without chemical modification (with reduced cost in manufacturing) still showed high levels of stability, translation efficiency, and immunogenicity. On the other hand, our algorithm is *orthogonal* to chemical modification and can be combined with it once the corresponding energy model is available. By unleashing the previously inaccessible region of highly stable and efficient sequences, LinearDesign is a timely and promising tool for mRNA vaccine development which is of utmost importance to the current and future pandemics. But more importantly, it is also a general and principled method for molecule design in mRNA medicine, and can be used for all therapeutic proteins including monoclonal antibodies and anti-cancer drugs.

References

1. Baden LR, et al. (2021) Efficacy and safety of the mRNA-1273 SARS-CoV-2 vaccine. *New England Journal of Medicine* 384(5):403–416.
2. Polack FP, et al. (2020) Safety and efficacy of the BNT162b2 mRNA Covid-19 vaccine. *New England Journal of Medicine*.

²CureVac does not use modification either, but uses codon optimization and engineers the non-coding regions (3); our algorithm is orthogonal to, and can be used with, their engineering efforts.

3. Gebre MS, et al. (2021) Optimization of non-coding regions for a non-modified mRNA COVID-19 vaccine. *Nature* pp. 1–8.
4. Crommelin DJ, Anchordoquy TJ, Volkin DB, Jiskoot W, Mastrobattista E (2021) Addressing the cold reality of mRNA vaccine stability. *Journal of Pharmaceutical Sciences* 110(3):997–1001.
5. Mauger DM, et al. (2019) mRNA structure regulates protein expression through changes in functional half-life. *Proceedings of the National Academy of Sciences U.S.A.* 116(48):24075–24083.
6. Hall KB (2005) *Best-first Word-lattice Parsing: Techniques for integrated syntactic language modeling*. (Brown University).
7. Schlake T, et al. (2019) mRNA: a novel avenue to antibody therapy? *Molecular Therapy* 27(4):773–784.
8. Reinhard K, et al. (2020) An RNA vaccine drives expansion and efficacy of claudin-CAR-T cells against solid tumors. *Science* 367(6476):446–453.
9. Wolff JA, et al. (1990) Direct gene transfer into mouse muscle in vivo. *Science* 247(4949):1465–1468.
10. Pardi N, Hogan MJ, Porter FW, Weissman D (2018) mRNA vaccines—a new era in vaccinology. *Nature Reviews Drug Discovery* 17(4):261–279.
11. Kon E, Elia U, Peer D (2021) Principles for designing an optimal mRNA lipid nanoparticle vaccine. *Current Opinion in Biotechnology* 73:329–336.
12. Gustafsson C, Govindarajan S, Minshull J (2004) Codon bias and heterologous protein expression. *Trends in Biotechnology* 22(7):346–353.
13. Nabiyouni M, Prakash A, Fedorov A (2013) Vertebrate codon bias indicates a highly GC-rich ancestral genome. *Gene* 519(1):113–119.
14. Sahin U, Karikó K, Türeci Ö (2014) mRNA-based therapeutics—developing a new class of drugs. *Nature reviews Drug discovery* 13(10):759–780.

15. Sharp PM, Li WH (1987) The codon adaptation index—a measure of directional synonymous codon usage bias, and its potential applications. *Nucleic Acids Research* 15(3):1281–1295.
16. Durbin R, Eddy SR, Krogh A, Mitchison G (1998) *Biological Sequence Analysis: Probabilistic Models of Proteins and Nucleic Acids*. (Cambridge University Press, Cambridge, UK).
17. Bar-Hillel Y, Perles M, Shamir E (1961) On formal properties of simple phrase structure grammars. *Zeitschrift für Phonetik, Sprachwissenschaft und Kommunikationsforschung* 14(2):143–172.
18. Cohen B, Skiena S (2003) Natural selection and algorithmic design of mRNA. *Journal of Computational Biology* 10(3-4):419–432.
19. Terai G, Kamegai S, Asai K (2016) CDSfold: an algorithm for designing a protein-coding sequence with the most stable secondary structure. *Bioinformatics* 32(6):828–834.
20. Huang L, et al. (2019) LinearFold: linear-time approximate RNA folding by 5'-to-3' dynamic programming and beam search. *Bioinformatics* 35(14):i295–i304.
21. Consortium U (2005) UniProt: a hub for protein information. *Nucleic Acids Research* 42:D204–D12.
22. Wrapp D, et al. (2020) Cryo-EM structure of the 2019-nCoV spike in the prefusion conformation. *Science* 367(6483):1260–1263.
23. Huang L, Chiang D (2005) Better k-best parsing. *Proceedings of the Ninth International Workshop on Parsing Technologies* pp. 53–64.
24. Liu L, et al. (2008) Structural basis of toll-like receptor 3 signaling with double-stranded RNA. *Science* 320(5874):379–381.
25. Mignone F, Gissi C, Liuni S, Pesole G (2002) Untranslated regions of mRNAs. *Genome biology* 3(3):1–10.

26. Jeong DE, et al. (2021) Assemblies of putative SARS-CoV2-spike-encoding mRNA sequences for vaccines BNT-162b2 and mRNA-1273 (version 0.1 beta 03/23/21).
27. Turner DH, Mathews DH (2010) NNDB: the nearest neighbor parameter database for predicting stability of nucleic acid secondary structure. *Nucleic Acids Research* 38(suppl_1):D280–D282.
28. Rana MM (2021) Polymer-based nano-therapies to combat COVID-19 related respiratory injury: progress, prospects, and challenges. *Journal of Biomaterials Science, Polymer Edition* pp. 1–31.
29. Karikó K, et al. (2008) Incorporation of pseudouridine into mRNA yields superior nonimmunogenic vector with increased translational capacity and biological stability. *Molecular Therapy* 16(11):1833–1840.

Availability

Web server: <http://rna.baidu.com>. Please contact rna@baidu.com if you need more advanced features.

Author Contributions

L.H. conceived and directed the project. L.H. designed the basic algorithm for the Nussinov model and wrote a Python prototype, and H.Z. and L.Z. extended this algorithm to the Turner model, and implemented it in C++, which Z.L. optimized. L.H., H.Z., and L.Z. designed the CAI integration algorithm which L.Z. and H.Z. implemented. L.Z. implemented the beam search and k -best modules, and handled design constraints. K.L. made the webserver. B.L. implemented a baseline. Y.Z. supervised the *in vitro* and *in vivo* experiments. A.L., X.M., F.Z. performed the protein expression and immunogenicity assays, and C.X. performed chemical stability and structure compactness assays. D.H.M. discussed the approach and provided guidance for *in silico* analysis and writing. L.H., H.Z., L.Z., D.H.M., A.L., C.X., and Y.Z. wrote the manuscript. The work of H.Z., L.Z., K.L., and L.H. were done at Baidu Research USA.

Acknowledgments

We thank Rhiju Das (Stanford) for introducing the mRNA design problem to us, Robin Li (Baidu) for connecting Baidu Research with Stemirna, Julia Li (Baidu Research) for coordinating resources for this project, Goro Terai and Kiyoshi Asai (Univ. of Tokyo) for sending us the CDSfold code, Sharon Aviran (UC Davis) for spotting a typo in the hyperparameter λ in our earlier version, Alicia Solórzano (Pfizer) for the question on LinearDesign's independence of the choice of UTRs, Jinzhong Lin (Fudan) for early discussions, and Sizhen Li (Oregon State Univ.) for proofreading and help on L^AT_EX. We thank Sanofi and many other vaccine companies worldwide for licensing and early adoption of LinearDesign. D.H.M. is supported by National Institutes of Health grant R01GM076485.

Methods

§1 Details of LinearDesign Algorithm

§1.1 Optimization Objectives There are two objectives in mRNA design: stability and codon optimality. The optimal-stability mRNA design problem can be formalized as follows. Given a protein sequence $\mathbf{p} = p_0 \dots p_{|\mathbf{p}|-1}$ where each p_i is an amino acid residue, we find the optimal mRNA sequence $\mathbf{r}^*(\mathbf{p})$ that has the *lowest minimum folding free energy change* (MFE) among all possible mRNA sequences encoding that protein:

$$\mathbf{r}^*(\mathbf{p}) = \operatorname{argmin}_{\mathbf{r} \in mRNA(\mathbf{p})} \text{MFE}(\mathbf{r}) \quad (1)$$

$$\text{MFE}(\mathbf{r}) = \min_{\mathbf{s} \in \text{structures}(\mathbf{r})} \Delta G^\circ(\mathbf{r}, \mathbf{s}) \quad (2)$$

where $mRNA(\mathbf{p}) = \{\mathbf{r} \mid \text{protein}(\mathbf{r}) = \mathbf{p}\}$ is the set of candidate mRNA sequences, $\text{structures}(\mathbf{r})$ is the set of all possible secondary structures for mRNA sequence \mathbf{r} , and $\Delta G^\circ(\mathbf{r}, \mathbf{s})$ is the free energy change of structure \mathbf{s} for mRNA \mathbf{r} according to an energy model. This is clearly a double minimization objective involving the per-sequence minimization over all of its possible structures (i.e., RNA folding; Eq. 2) which has well-known dynamic programming solutions, and the global minimization over all sequences (i.e., optimal mRNA design; Eq. 1) which we will solve using lattice parsing (§1.3).

Next, we integrate codon optimality by adding Codon Adaptation Index (CAI) (1), defined as the geometric mean of the codon optimality of each codon in the mRNA \mathbf{r} :

$$\text{CAI}(\mathbf{r}) = \sqrt[|\mathbf{r}|]{\prod_{0 \leq i < \frac{|\mathbf{r}|}{3}} w(\text{codon}(\mathbf{r}, i))}$$

where $\text{codon}(\mathbf{r}, i) = r_{3i}r_{3i+1}r_{3i+2}$ is the i th triplet codon in \mathbf{r} , and $w(c)$ is the relative adaptiveness of codon c , defined as the frequency of c divided by the frequency of its most frequent synonymous codon ($0 \leq w(c) \leq 1$). Because CAI is always between 0 and 1 but MFE is generally proportional to the mRNA sequence length, we scale CAI by the number of codons and use a hyperparameter λ to balance MFE and CAI ($\lambda = 0$ being purely MFE), and define a novel joint objective:

$$\text{MFECAI}_\lambda(\mathbf{r}) = \text{MFE}(\mathbf{r}) - \frac{|\mathbf{r}|}{3} \lambda \log \text{CAI}(\mathbf{r})$$

which can be simplified by expanding CAI:

$$\begin{aligned}
\text{MFECAI}_\lambda(\mathbf{r}) &= \text{MFE}(\mathbf{r}) - \frac{|\mathbf{r}|}{3} \lambda \log \sqrt[|\mathbf{r}|/3]{\prod_{0 \leq i < \frac{|\mathbf{r}|}{3}} w(\text{codon}(\mathbf{r}, i))} \\
&= \text{MFE}(\mathbf{r}) - \lambda \sum_{0 \leq i < \frac{|\mathbf{r}|}{3}} \log w(\text{codon}(\mathbf{r}, i))
\end{aligned} \tag{3}$$

This joint objective is basically MFE plus (a scaled) sum of the negative logarithm of each codon's relative adaptiveness. Now the joint optimization can be defined as:

$$\mathbf{r}_\lambda^*(\mathbf{p}) = \underset{\mathbf{r} \in mRNA(\mathbf{p})}{\text{argmin}} \text{MFECAI}_\lambda(\mathbf{r}) = \underset{\mathbf{r} \in mRNA(\mathbf{p})}{\text{argmin}} \left(\text{MFE}(\mathbf{r}) - \lambda \sum_{0 \leq i < \frac{|\mathbf{r}|}{3}} \log w(\text{codon}(\mathbf{r}, i)) \right)$$

See Fig. 2D for examples of relative adaptiveness calculation.

§1.2 DFA Representations for Codons and mRNA Candidate Sequences

Informally, a DFA is a directed graph with labeled edges and distinct start and end states. For our purpose each edge is labeled by a nucleotide, so that for each codon DFA, each start-to-end path represents a triplet codon. Formally, a DFA is a 5-tuple $\langle Q, \Sigma, \delta, q_0, F \rangle$, where Q is the set of states, Σ is the alphabet (here $\Sigma = \{A, C, G, U\}$), q_0 is the start state (always (0,0) in this work), F is the set of end states (in this work the end state is unique, i.e., $F = \{(3,0)\}$), and δ is the transition function that takes a state q and a symbol $a \in \Sigma$ and returns the next state q' , i.e., $\delta(q, a) = q'$ encodes a labeled edge $q \xrightarrow{a} q'$.

After building DFAs for each amino acid, we can concatenate them into a single DFA $D(\mathbf{p})$ for a protein sequence \mathbf{p} , which represents all possible mRNA sequences that translate into that protein

$$D(\mathbf{p}) = D(p_0) \circ D(p_1) \circ \dots \circ D(p_{|\mathbf{p}|-1}) \circ D(\text{STOP})$$

by stitching the end state of each DFA with the start state of the next. The new end state of the mRNA DFA is $(3|\mathbf{p}|+3, 0)$.

We also define $out_edges(q)$ to be the set of outgoing edges from state q , and $in_edges(q)$ to be the set of incoming edges (which will be used in the pseudocode, see Figs. S3–S4):

$$\begin{aligned}
out_edges(q) &= \{q \xrightarrow{a} q' \mid \delta(q, a) = q'\} \\
in_edges(q) &= \{q' \xrightarrow{a} q \mid \delta(q', a) = q\}
\end{aligned}$$

For the mRNA DFA in Fig. S2D, $out_edges((3,0)) = \{(3,0) \xrightarrow{U} (4,0), (3,0) \xrightarrow{C} (4,1)\}$ and $in_edges((9,0)) = \{(8,0) \xrightarrow{A} (9,0), (8,0) \xrightarrow{G} (9,0), (8,1) \xrightarrow{A} (9,0)\}$.

§1.3 Objective 1 (Stability): Stochastic Context-Free Grammar, Lattice Parsing, and Intersection

A stochastic context-free grammar (SCFG) is a context-free grammar in which each rule is augmented with a weight. More formally, an SCFG is a 4-tuple $\langle N, \Sigma, P, S \rangle$ where N is the set of non-terminals, Σ is the set of terminals (identical to the alphabet in the DFA, in this case $\Sigma = \{A, C, G, U\}$), P is the set of weight-associated context-free writing rules, and $S \in N$ is the start symbol. Each rule in P has the form $A \xrightarrow{w} (N \cup \Sigma)^*$ where $A \in N$ is a non-terminal that can be rewritten according to this rule into a sequence of non-terminals and terminals (the star $*$ means repeating zero or more times) and $w \in \mathbb{R}$ is the weight associated with this rule.

SCFGs are commonly used to represent the RNA folding energy model. The weight of a derivation (parse tree, or a secondary structure in this case) is the sum of weights of the productions used in that derivation (2). For example, for a very simple Nussinov-Jacobson-style model (3), which simplifies the energy model to individual base pairs, we can define this SCFG G as in Fig. S2E, where each GC pair gets a score of -3 , and each AU pair gets a score of -2 . Thus, the standard RNA secondary structure prediction problem can be cast as a parsing problem: given the above SCFG G and an input RNA sequence, find the minimum-weight derivation in G that can generate the sequence. This can be solved by the classical CKY algorithm from computational linguistics (4-6).

The optimal-stability mRNA design problem is now a simple extension of the above single-sequence folding problem to the case of multiple inputs: instead of finding the minimum free energy structure (minimum weight derivation) for a given sequence, we find the minimum free energy structure (and its corresponding sequence) among all possible structures for all possible sequences (see Fig. S2). This can be solved by lattice parsing on the DFA, which is a generalization of CKY from a single sequence to a DFA. Take the bifurcation rule $S \rightarrow NP$ for example. In CKY, if you have derived non-terminal N for span $[i, j]$, notated $i \xrightarrow{\Delta^N} j$, and if you have also derived $j \xrightarrow{\Delta^P} k$, you can combine the two spans, i.e., $i \xrightarrow{\Delta^N} j \xrightarrow{\Delta^P} k$, and use the above rule to derive $i \xrightarrow{\Delta^S} k$. Similarly, in lattice parsing, if you have derived both $q_i \xrightarrow{\Delta^N} q_j$ (i.e., there is a $q_i \rightsquigarrow q_j$ path that can be derived from N) and $q_j \xrightarrow{\Delta^P} q_k$, you can combine them to a longer path $q_i \xrightarrow{\Delta^N} q_j \xrightarrow{\Delta^P} q_k$ and derive $q_i \xrightarrow{\Delta^S} q_k$ with the above rule. While the runtime for CKY scales $O(|G|n^3)$ where $|G|$ is the grammar constant (the number of rules) and n is the RNA sequence length, the runtime for lattice

parsing similarly scales $O(|G||D|^3)$ where $|D|$ is the number of states in the DFA. For mRNA design with the standard genetic code, $n \leq |D| \leq 2n$ because each position i has either one or two states $((i, 0)$ and $(i, 1))$, so its time complexity is also actually identical to single-sequence folding, just with a larger constant. See Methods §1.6 for details of this algorithm and Figs. S3–S4 for the pseudocode.

More formally, in theoretical computer science, lattice parsing with an CFG G on a DFA D is also known as the intersection between the languages of G and D (i.e., the sets of sequences allowed by G and D), notated $L(G) \cap L(D)$, which was solved by the Bar-Hillel construction in 1961 (7). In order to adapt it to mRNA design, we need to extend this concept to the case of weighted (i.e., stochastic) grammars and weighted DFAs (the latter is needed for CAI integration; see below). While the language $L(G)$ of CFG G is the set of sequences generated by G , the language of the SCFG for RNA folding free energy model defines a mapping from each RNA sequence to its MFE, i.e., $L_w(G) : \Sigma^* \mapsto \mathbb{R}$. This can be written as a relation:

$$L_w(G) = \{\mathbf{r} \sim \text{MFE}(\mathbf{r}) \mid \mathbf{r} \in \Sigma^*\}$$

And we also extend the language of a DFA to a trivial weighted language (which will facilitate the incorporation of CAI into DFA below):

$$L_w(D) = \{\mathbf{r} \sim 0 \mid \mathbf{r} \in L(D)\}$$

Next we extend the intersection from two sets to two weighted sets A and B :

$$A \cap_w B = \{\mathbf{r} \sim (w_1 + w_2) \mid \mathbf{r} \sim w_1 \in A, \mathbf{r} \sim w_2 \in B\}$$

Now we can show that optimal-stability mRNA design problem can be solved via weighted intersection between $L_w(G)$ and $L_w(D)$, i.e., we can construct a new “intersected” stochastic grammar G' that has the same weights (i.e., energy model) as the original grammar but only generates sequences in the DFA:

$$L_w(G') = L_w(G) \cap_w L_w(D) = \{\mathbf{r} \sim \text{MFE}(\mathbf{r}) \mid \mathbf{r} \in L(D)\}$$

§1.4 Adding Objective 2 (Codon Optimality): Weighted DFA for CAI Integration As described in the main text and Fig. 2D, our novel joint optimization objective (Eq. 3) factors the CAI of each mRNA candidate onto the relative adaptiveness

of each of its codons, and thus can be easily incorporated into the DFA as edge weights. To do this we need to extend the definition of DFA to weighted DFA, where the transition function δ now returns a state and a weight, i.e., $\delta(q, a) = (q', w)$, which encodes a weighted label edge $q \xrightarrow{a:w} q'$. Now the set of outgoing and incoming edges are also updated to:

$$\begin{aligned} out_edges(q) &= \{q \xrightarrow{a:w} q' \mid \delta(q, a) = (q', w)\} \\ in_edges(q) &= \{q' \xrightarrow{a:w} q \mid \delta(q', a) = (q, w)\} \end{aligned}$$

In this case, the weighted DFA defines a mapping from each candidate mRNA sequence to its negative logarithm of CAI scaled by the number of codons, i.e., $L_w(D) : L(D) \mapsto \mathbb{R}$. More formally,

$$L_w(D) = \{\mathbf{r} \sim -\frac{|\mathbf{r}|}{3} \log \text{CAI}(\mathbf{r}) \mid \mathbf{r} \in L(D)\}$$

Now the weighted intersection defined above can be extended to incorporate the hyperparameter λ and derive the joint objective:

$$L_w^\lambda(G') = L_w(G) \cap_w^\lambda L_w(D) = \{\mathbf{r} \sim (\text{MFE}(\mathbf{r}) - \lambda \frac{|\mathbf{r}|}{3} \log \text{CAI}(\mathbf{r})) \mid \mathbf{r} \in L(D)\}$$

§1.5 Bottom-Up Dynamic Programming Next, we describe how to implement the dynamic programming algorithm behind lattice parsing (or equivalently, intersection between the languages of a stochastic context-free grammar and a weighted DFA) to solve the joint optimization problem. For simplicity reasons, here we use bottom-up dynamic programming on a modified Nussinov-Jacobson energy model. Fig. S3 gives the pseudocode for this simplified version. We first build up the mRNA DFA for the given protein, and initialize two hash tables, *best* to store the best score of each state, and *back* to store the best backpointer. For the base cases ($S \xrightarrow{0} N N N$), we set $best[S, q_i, q_{i+3}] \leftarrow 0$ for optimal-stability design, and $best[S, q_i, q_{i+3}] \leftarrow \text{mincost}(q_i, q_{i+3}, \lambda)$ for the joint optimization where

$$\text{mincost}(q_i, q_{i+3}, \lambda) \triangleq \min_{q_i \xrightarrow{a:w_1} q' \xrightarrow{b:w_2} q'' \xrightarrow{c:w_3} q_{i+3}} \lambda(w_1 + w_2 + w_3) \quad (4)$$

is the minimum (λ -scaled) cost of any $q_i \rightsquigarrow q_{i+3}$ path in the CAI-integrated DFA. Next, for each state (q_i, q_j) it goes through the pairing rule and bifurcation rules, and updates if a better score is found. After filling out the hash tables bottom-up, we can backtrack the best mRNA sequence stored with the backpointers. See Fig. S4 for details of UPDATE and BACKTRACE functions.

§1.6 Left-to-Right Dynamic Programming and Beam Search Inspired by our previous work, LinearFold (8), we further developed a linear-time approximation algorithm for mRNA design. We apply beam pruning (9), a classical pruning technique, to significantly narrow down the search space without sacrificing too much search quality.

Fig. S5 gives the pseudocode of simplified LinearDesign algorithm for the Nussinov model, based on left-to-right dynamic programming and beam pruning. LinearDesign replaces bottom-up dynamic programming with a left-to-right parsing. At each step j (the j th position of mRNA sequence), we only keep the top b states with the lowest cost and prune out the less promising states, since they are unlikely to be the optimal sequence. Here b , the beam size, is a user-adjustable parameter to balance runtime and search quality. Notice that we use $b = 100$ as default in LinearFold (20), but in LinearDesign we usually use a larger beam size of $b = 500$ because the search space is larger.

Our real system uses a left-to-right dynamic programming with beam pruning on the Turner nearest neighbor free energy model (10, 11). We implement the thermodynamic parameters following Vienna RNAfold (12), except for the dangling ends. Dangling ends refer to stabilizing interactions for multiloops and external loops (13), which require knowledge of the nucleotide sequence outside of the state (q_i, q_j) . Though it could be integrated in LinearDesign, the implementation becomes more involved.

§1.7 DFAs for Other Genetic Codes, Coding Constraints, and Modified Nucleotides The DFA framework can also represent less common cases such as alternative genetic codes, modified nucleotides, and coding constraints. First, DFA can encode non-standard genetic codes, such as alternative nuclear code for some yeast (14) and mitochondrial codes (15) (Fig. S6A). Second, we may want to avoid some unwanted or rare codons (such as the amber stop codon) which is an easy change on the codon DFAs (Fig. S6B), or certain adjacent codon pairs that modulate translation efficiency (16), which is beyond the scope of single codon DFAs but easy on the mRNA DFA (Fig. S6C). Similarly, we may want to disallow certain restriction enzyme recognition sites, which span across multiple codons (S7). Finally, chemically modified nucleotides such as pseudouridine (Ψ) have been widely used in mRNA vaccines (17), which can also be incorporated in the DFA (Fig. S6D).

§1.8 Related Work Two previous studies also tackled our objective 1 (optimal-stability mRNA design) via dynamic programming, but their algorithms are ad-hoc and complicated (18, 19). By contrast, our work solves the harder and more general problem of joint optimization between stability and codon optimality (which subsumes their objective as a special case), yet using a much simpler and extendable solution. First, our work is the first to use automata theory to compactly and conveniently represent the exponentially large mRNA design space. Second, our reduction of mRNA design to lattice parsing induces a simple yet efficient solution based on classical results in computational linguistics and theoretical computer science, which scales $O(n^2)$ rather than $O(n^3)$ for practical applications (Figs. 3 & S8). Third, we define a novel joint optimization objective that factors the (logarithm of) CAI of an mRNA *additively* onto its individual codons, making it possible to incorporate codon optimality into dynamic programming. Codon usage is an important factor in mRNA design (20) that previous work was unable to jointly optimize.³ Fourth, our DFA framework is so general that it can also represent arbitrary (non-standard) genetic codes, modified nucleotides, and coding constraints such as adjacent codon pair preference, which previous work could not handle even with major modifications. Fifth, we further develop a faster, linear-time, approximate version which greatly reduces runtime for long sequences with small sacrifices in search quality, which we also use to generate multiple suboptimal candidates with varying folding stability and codon optimality as candidates for experimentation. Last but not least, extensive experiments confirm that compared to the standard codon optimization benchmark, our designs are substantially better in chemical stability and protein expression *in vitro*, and the corresponding mRNA vaccines elicit up to 23× higher antibody responses *in vivo* (see Fig. 4).

§1.9 Benchmark Dataset and Machine To estimate the time complexity of LinearDesign, we collected 114 human protein sequences from UniProt (21), with length from 78 to 3,333 amino acids (not including the stop codon). We benchmarked LinearDesign on a Linux machine with 2 Intel Xeon E5-2660 v3 CPUs (2.60 GHz) and 377 GB memory, and used Clang (11.0.0) to compile.

³CDSfold (19) uses simulated annealing to improve CAI by fine-tuning from the MFE solution, but this is a heuristic with no guarantees, and their objective formulation, unlike ours, does not factor onto individual codons, thus cannot be incorporated into dynamic programming.

§1.10 Additional Design Constraints Some studies have shown that protein expression level drops if the 5'-end leader region has more secondary structure (20, 22–25). To design sequences with less structures at 5'-end leader region, we take a simple “design, enumerate and concatenate” strategy to loose structure of the leader region: (1) design the CDS region except for the 5'-end leader region (i.e., the first 15 nucleotides); (2) enumerate all possible subsequences in the 5'-end leader region; and (3) concatenate each subsequence with the designed sequence, refold, and choose the one whose 5'-end leader region has the most unpaired nucleotides.

In addition, it has been revealed that long double-stranded region may induce unwanted innate immune responses by previous studies (26–28). Considering this, we do not allow long double-stranded regions that include 33 or more base pairs in our design algorithms.

§2 Details of *In vitro* and *In vivo* Experiments

§2.1 Preparation of mRNA Vaccine mRNA molecules were synthesized from corresponding linearized plasmid DNA template using T7 RNA polymerase, which flanked the open-reading frame (ORF) of Spike antigen with the 5' and 3' untranslated regions and a 70 *nt* poly-A tail. Cleancap analog was included to obtain capped RNA. The transcription reaction was incubated at 37°C for 6–8 hours, followed by treatment with DNase. RNA was then purified using Carboxylated microspheres. For the preparation of mRNA vaccines, lipopolyplex delivery platform was used to encapsulate the mRNA cargo as previously reported (29).

§2.2 Electrophoretic Mobility Shift Assay (EMSA) and Integrity assay of mRNA To compare the electrophoretic mobility of mRNA molecules, mRNA samples were stored in Ambion® RNA storage buffer (Cat. # AM7001, Thermo Fisher, $Mg^{2+} = 0mM$). After denaturing at 70°C for 5 mins followed by cooling on ice, the mRNA samples were loaded on 1% agrose gel to run at 130V for 1h at 4°C. Gel image was taken by Gel Doc XR+ Gel Documentation System (Bio-Rad). (Fig. 4B)

RNA integrity was assayed by Qsep100™ Capillary Electrophoresis System. Intact mRNA was calculated as the percentage of full-length mRNA in solution. (Fig. 4C)

§2.3 Protein Expression Assay

Cell Culture Human embryonic kidney (HEK)293T cells were cultured in Dulbecco’s modified Eagle’s medium (DMEM) (Hyclone) containing 10% fetal bovine serum (FBS) (GEMINI) and 1% Penicillin-Streptomycin (Gibco). All cells were cultured at 37°C in a 5% CO₂ condition.

Measurement of Protein Expression from mRNA Cells were transfected with mRNA molecules using Lipofectamine MessengerMAX (Thermo Scientific). Briefly, 2 μ g of mRNA was mixed with 6 μ L of Lipofectamine reagent first and then incubated with cells for 24 or 48 hours. For flow cytometric analysis, cells were collected and stained with live/dead cell dye (Fixable Viability Stain 510, BD) for 5 min. After washing, cells were incubated with anti-RBD chimeric mAb (1:100 dilution, Sino Biological) for 30 min, followed by washing and incubation with PE-anti-human IgG Fc (1:100 dilution, Biogend) for 30 min. Samples were then acquired on BD Canto II (BD Biosciences). Data were analyzed using FlowJo V10.1 (Tree Star). (Fig. 4A and D)

§2.4 Immunization C57BL/6 mice (6-8 weeks) were intramuscularly immunized twice with 10 μ g of mRNA vaccines at a 2-week interval. Sera and spleens were collected 14 days after boost immunization. All experiments using mouse model were conducted under the ethical regulations and were approved by local ethical committees.

Surrogate Virus Neutralization (sVNT) Assay (Neutralizing Antibody Assay) Neutralizing antibody titer was measured using sVNT assay as previously reported (30) with some modifications. Briefly, 96-well plates (Greiner Bio-one) were coated with hACE2 protein (100ng/well, Genscript) overnight at 4°C. Plates were washed with PBST and blocked with 2% BSA for 2 hours at RT. HRP-conjugated RBD (100 ng/ml) were incubated with serially diluted serum from immunized mice at an equal volume (60 μ L each) for 30 min at 37°C. Sera collected from mice receiving PBS injection were used as negative control. Following this, a 100- μ L mixture of RBD and serum was added into each well and incubated for 15 min at 37°C. After washing, TMB substrate (Invitrogen) was used for development and the absorbance was read at 450 nm using BioTek

microplate reader. The IC50 value was calculated using 4 parameter logistic non-linear regression. (Fig. 4E)

Enzyme-linked Immunosorbent Assays (Binding Antibody Assay) Recombinant SARS-CoV-2 Spike ectodomain protein (100 ng/well, Genscript) diluted in coating buffer (Biolegend) were coated into 96-well EIA/RIA plates (Greiner Bio-one) overnight at 4°C. The plates were then washed with PBS-T (0.05% Tween-20) and were blocked with 2% BSA in PBST for 2 hours at room temperature (RT). Serum samples (1:6400 diluted) were added and incubated for 2 hours at RT. After washing, total IgG was evaluated using HRP-conjugated goat anti-mouse IgG Ab (1:10,000) for 1 hour. TMB substrate (Invitrogen) was used for development and the absorbance was read at 450 nm using BioTek microplate reader. (Fig. 4F)

Enzyme-linked Immunospot (ELISpot) Assay (T Cell Response Assay) Frequency of Spike antigen-specific IFN- γ -secreting T cells was evaluated using Mouse IFN- γ ELISpotplus Kit (Mabtech) according to the manual. Briefly, 3×10^5 murine splenocytes were added to wells pre-coated with anti-mouse IFN- γ capturing Abs and were incubated with Spike protein (10 $\mu\text{g}/\text{ml}$) for 20 hours. After washing, plates were incubated with Streptavidin-ALP (1:1000) for 1 hour at RT. Spots were developed with BCIP/NBT substrate solution and counted using Immunospot S6 analyzer (CTL). (Fig. 4G)

Supplementary Figures and Tables

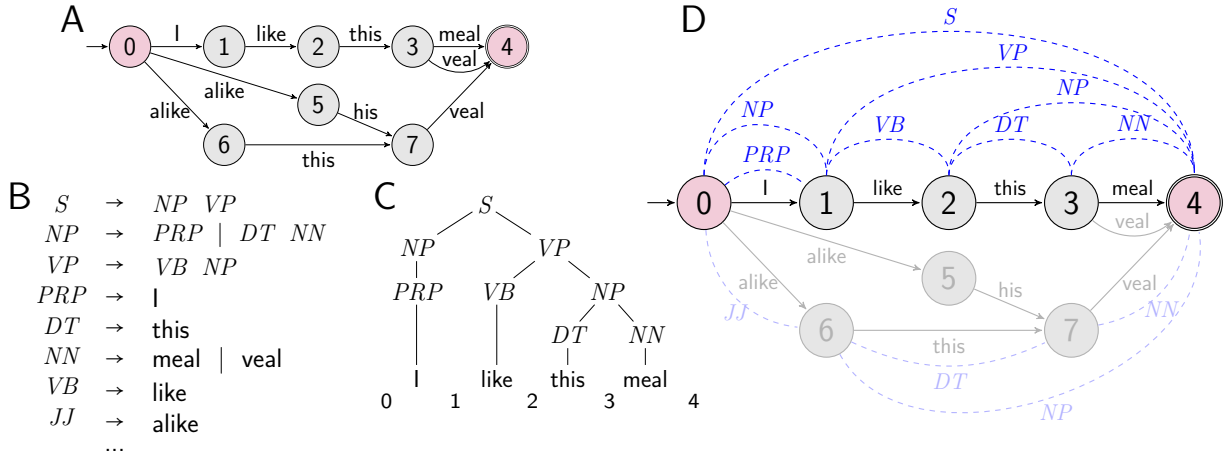


Figure S1: The word lattice parsing in natural language processing. **A**: An example of word lattice (sentence DFA) for speech recognition. **B**: Simplified language grammar. **C**: Single sentence parsing with between-word indices, which is a special case of word lattice parsing. **D**: Illustration of word lattice parsing for speech recognition with given word lattice and language grammar; the dashed blue arcs above the DFA depict the best parsing structure for the optimal sentence “I like this meal”, while the dashed light-blue arcs below the DFA represent the best parsing structure for a non-optimal sentence “alike this veal”. See also Fig. 1.

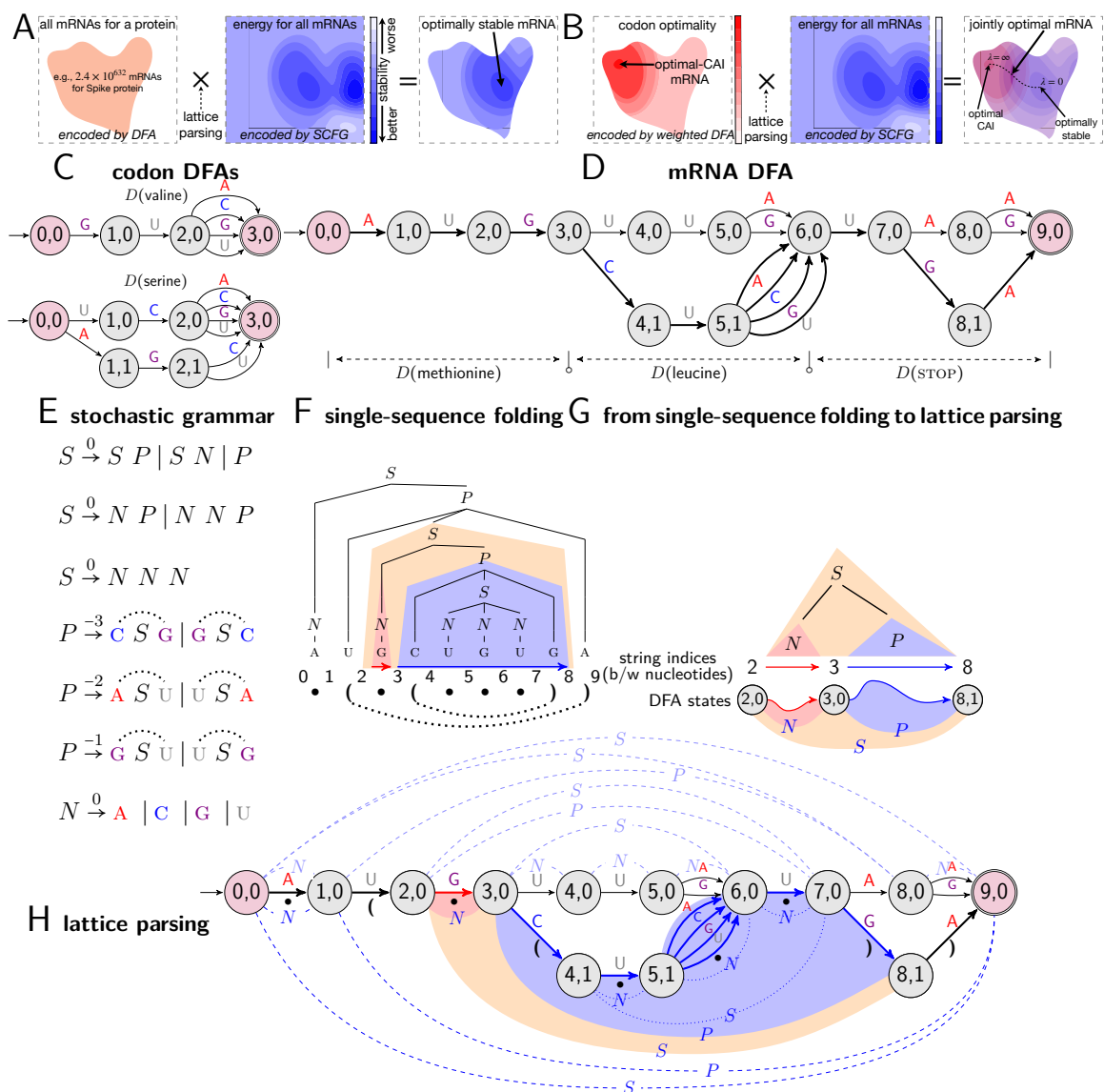


Figure S2: **A–B**: Illustrations of mRNA design as optimization problems for stability (objective 1, in **A**) and joint stability and codon optimality (objectives 1 & 2, in **B**). **C–H** show how lattice parsing solves the first optimization problem (see Fig. 2D for the second). **C**: Codon DFAs. **D**: An mRNA DFA made of three codon DFAs. The thick paths depict the optimal mRNA sequences under the simplified energy model in **E**, AUGCU*UGA, where * could be any nucleotide. **E**: Stochastic context-free grammar (SCFG) for a simplified folding free energy model. Each rule has a cost (i.e., energy term, the lower the better), and the dotted arcs represent base pairs in RNA secondary structure. **F**: Single-sequence folding is equivalent to context-free parsing with an SCFG; the parse tree represents the best secondary structure for the input mRNA sequence. **G**: We extend single-sequence parsing (top) to lattice parsing (bottom) by replacing the input string with a DFA, where each string index becomes a DFA state, and a span becomes a path between two states. **H**: Lattice parsing with the grammar in **E** for the DFA in **D**. The blue arcs below the DFA depict the (shared) best structure for the optimal sequences AUGCU*UGA in the whole DFA, while the dashed light-blue arcs above the DFA represent the best structure for a suboptimal sequence AUGUUAUAA. Lattice parsing can also incorporate codon optimality (objective 2, see **B**), by replacing the DFA with a weighted one (Fig. 2D).

```

1: function BOTTOMUPDESIGN(p,  $\lambda$ )           ▷ p: protein sequence;  $\lambda$ : weight of CAI
2:    $n \leftarrow 3 \cdot (|\mathbf{p}| + 1)$            ▷ mRNA length; +1 for the stop codon
3:    $D \leftarrow D(x_1) \circ D(x_2) \circ \dots \circ D(\text{stop})$    ▷ build (CAI-integrated) mRNA DFA
4:    $best \leftarrow \text{hash}()$                  ▷ hash table: from  $[X, q_i, q_j]$  to score
5:    $back \leftarrow \text{hash}()$                ▷ hash table: from  $[X, q_i, q_j]$  to backpointer
6:   for  $i = 0 \dots (n - 3)$  do             ▷ base case:  $S \xrightarrow{0} N N N$ 
7:     for each  $q_i \in \text{nodes}(D, i)$  do
8:       for each  $q_{i+3} \in \text{nodes}(D, i + 3)$  do
9:          $best[S, q_i, q_{i+3}] \leftarrow \text{mincost}(q_i, q_{i+3}, \lambda)$  ▷ best cost of any  $q_i \rightsquigarrow q_{i+3}$  path (Eq. 4)
10:    for  $l = 2 \dots n$  do                 ▷  $l = (j - i)$  is the span width
11:      for  $i = 0 \dots (n - l)$  do
12:         $j \leftarrow i + l$ 
13:        for each  $q_i \in \text{nodes}(D, i)$  do
14:          for each  $q_j \in \text{nodes}(D, j)$  do
15:            for each  $q_{j-1} \xrightarrow{b:w_b} q_j \in \text{in\_edges}(D, q_j)$  do           ▷  $q_i \xrightarrow{S} q_{j-1} \xrightarrow{b} q_j$ 
16:              UPDATE( $S, q_i, q_j, best[S, q_i, q_{j-1}] + \lambda w_b, (q_{j-1}, b)$ )           ▷  $S \xrightarrow{0} S N$ 
17:              if  $j - i > 4$  then                 ▷ pairing (no sharp turn)
18:                for each  $q_i \xrightarrow{a:w_a} q_{i+1} \in \text{out\_edges}(D, q_i)$  do           ▷  $q_i \xrightarrow{a} q_{i+1} \xrightarrow{S} q_{j-1} \xrightarrow{b} q_j$ 
19:                  if  $\Delta G(a, b) < 0$  then           ▷  $\Delta G(C, G) = -3; \Delta G(A, U) = -2; \dots$ 
20:                     $score \leftarrow best[S, q_{i+1}, q_{j-1}] + \lambda(w_a + w_b) + \Delta G(a, b)$    ▷  $P \xrightarrow{-3} C S G | \dots$ 
21:                    UPDATE( $P, q_i, q_j, score, (a, q_{i+1}, q_{j-1}, b)$ )
22:                  for  $k = (i + 1) \dots (j - 1)$  do           ▷ bifurcation midpoint
23:                    for each  $q_k \in \text{nodes}(D, k)$  do           ▷  $q_i \xrightarrow{S} q_k \xrightarrow{P} q_j$ 
24:                       $score \leftarrow best[S, q_i, q_k] + best[P, q_k, q_j]$            ▷  $S \xrightarrow{0} S P$ 
25:                      UPDATE( $S, q_i, q_j, score, q_k$ )
26:    return  $best[S, q_0, q_n], \text{BACKTRACE}(S, q_0, q_n)$ 

```

Figure S3: The pseudocode of a simplified bottom-up version of our mRNA Design algorithm for the joint optimization between stability and codon optimality. The costs in blue are for CAI integration. See Methods §1.5 for more algorithm description, and Fig. S4 for UPDATE and BACKTRACE functions.

```

1: function UPDATE( $X, q_i, q_j, score, backpointer$ )
2:   if key ( $X, q_i, q_j$ ) not in  $best$  or  $score < best[X, q_i, q_j]$  then      ▷ minimizing weight
3:      $best[X, q_i, q_j] \leftarrow score$ 
4:      $back[X, q_i, q_j] \leftarrow backpointer$ 

1: function BACKTRACE( $X, q_i, q_j$ )      ▷ returns a (sequence, structure) pair
2:    $backpointer \leftarrow back[X, q_i, q_j]$ 
3:   if  $index(q_j) - index(q_i) = 3$  then      ▷  $index(q)$ : the string index of state  $q$ 
4:     return ANYPATH( $q_i, q_j$ ), "... "      ▷  $S \xrightarrow{0} N N N$ ; any  $q_i \rightsquigarrow q_j$  path is fine
5:   if  $length(backpointer) = 4$  then      ▷ pairing:  $P \xrightarrow{-3} C S G | \dots$ 
6:      $a, q_{i+1}, q_{j-1}, b \leftarrow backpointer$       ▷  $q_i \xrightarrow{a} q_{i+1} \xrightarrow{seq} q_{j-1} \xrightarrow{b} q_j$ 
7:      $seq, struct \leftarrow BACKTRACE(S, q_{i+1}, q_{j-1})$ 
8:     return  $a + seq + b, "(" + struct + ")"$ 
9:   else if  $length(backpointer) = 2$  then      ▷ skip:  $S \xrightarrow{0} S N$ 
10:     $q_{j-1}, b \leftarrow backpointer$       ▷  $q_i \xrightarrow{seq} q_{j-1} \xrightarrow{b} q_j$ 
11:     $seq, struct \leftarrow BACKTRACE(S, q_i, q_{j-1})$ 
12:    return  $seq + b, struct + "."$ 
13:   else      ▷ bifurcation:  $S \xrightarrow{0} S P$ 
14:     $q_k \leftarrow backpointer$       ▷  $q_i \xrightarrow{seq_1} q_k \xrightarrow{seq_2} q_j$ 
15:     $seq_1, struct_1 \leftarrow BACKTRACE(S, q_i, q_k)$ 
16:     $seq_2, struct_2 \leftarrow BACKTRACE(P, q_k, q_j)$ 
17:    return  $seq_1 + seq_2, struct_1 + struct_2$ 

1: function BEAMPRUNE( $X, j, b$ )
2:    $cands \leftarrow hash()$       ▷ hash table: from  $q_i$  to score  $best[S, q_0, q_i] + best[X, q_i, q_j]$ 
3:   for each  $q_j \in nodes(j)$  do
4:     for each key ( $X, q_i, q_j$ )  $\in best$  do
5:        $cands[q_i] \leftarrow best[S, q_0, q_i] + best[X, q_i, q_j]$       ▷  $best[S, q_0, q_i]$  as prefix score
6:    $cands \leftarrow SELECTTOPB(cands, b)$       ▷ select top- $b$  by score
7:   for each key ( $X, q_i, q_j$ )  $\in best$  do
8:     if key  $q_i$  not in  $cands$  then
9:       delete ( $X, q_i, q_j$ ) in  $best$       ▷ prune out low-scoring states

```

Figure S4: The pseudocode for UPDATE, BACKTRACE (used in BOTTOMUPDESIGN, see Fig. S3) and BEAMPRUNE (used in LINEARDESIGN, see Fig. S5) functions.

```

1: function LINEARDESIGN( $\mathbf{p}, \lambda, b$ ) ▷  $b$  is beam size
10: for  $j = 4 \dots n$  do
11:   for each  $q_{j-1} \in \text{nodes}(D, j-1)$  do
12:     for each  $q_i$  such that  $(S, q_i, q_{j-1}) \in \text{best}$  do
13:       for each  $q_{j-1} \xrightarrow{b:w_b} q_j \in \text{out\_edges}(D, q_{j-1})$  do ▷  $q_i \xrightarrow{S} q_{j-1} \xrightarrow{b} q_j$ 
14:         UPDATE( $S, q_i, q_j, \text{best}[q_i, q_{j-1}] + \lambda w_b, (q_{j-1}, b)$ ) ▷  $S \xrightarrow{0} S N$ 
15:         for each  $q_{i-1} \xrightarrow{a:w_a} q_i \in \text{in\_edges}(D, q_i)$  do ▷  $q_{i-1} \xrightarrow{a} q_i \xrightarrow{S} q_{j-1} \xrightarrow{b} q_j$ 
16:         if  $\Delta G(a, b) < 0$  then ▷  $\Delta G(C, G) = -3; \Delta G(A, U) = -2; \dots$ 
17:            $\text{score} \leftarrow \text{best}[S, q_i, q_{j-1}] + \lambda(w_a + w_b) + \Delta G(a, b)$ 
18:           UPDATE( $P, q_{i-1}, q_j, \text{score}, (a, q_i, q_{j-1}, b)$ ) ▷  $P \xrightarrow{-3} C S G | \dots$ 
19:     BEAMPRUNE( $P, j, b$ ) ▷ choose top- $b$  among all  $(P, q_i, q_j)$ 's
20:   for each  $q_j \in \text{nodes}(D, j)$  do
21:     for each  $q_i$  such that  $(P, q_i, q_j) \in \text{best}$  do
22:       for each  $q_k$  such that  $(S, q_k, q_i) \in \text{best}$  do
23:          $\text{score} \leftarrow \text{best}[S, q_k, q_i] + \text{best}[P, q_i, q_j]$  ▷  $q_i \xrightarrow{S} q_k \xrightarrow{P} q_j$ 
24:         UPDATE( $S, q_k, q_j, \text{score}, q_i$ ) ▷  $S \xrightarrow{0} S P$ 
25:     BEAMPRUNE( $S, j, b$ ) ▷ choose top- $b$  among all  $(S, q_i, q_j)$ 's
26: return  $\text{best}[S, q_0, q_n], \text{BACKTRACE}(S, q_0, q_n)$ 

```

Figure S5: The pseudocode of (simplified) LinearDesign algorithm for the joint optimization between stability and codon optimality. The costs in blue are for CAI integration. The first 9 lines are the same as in BOTTOMUPDESIGN (see Fig. S3). See Methods §1.6 for more algorithm description, and Fig. S4 for UPDATE, BACKTRACE, and BEAMPRUNE functions.

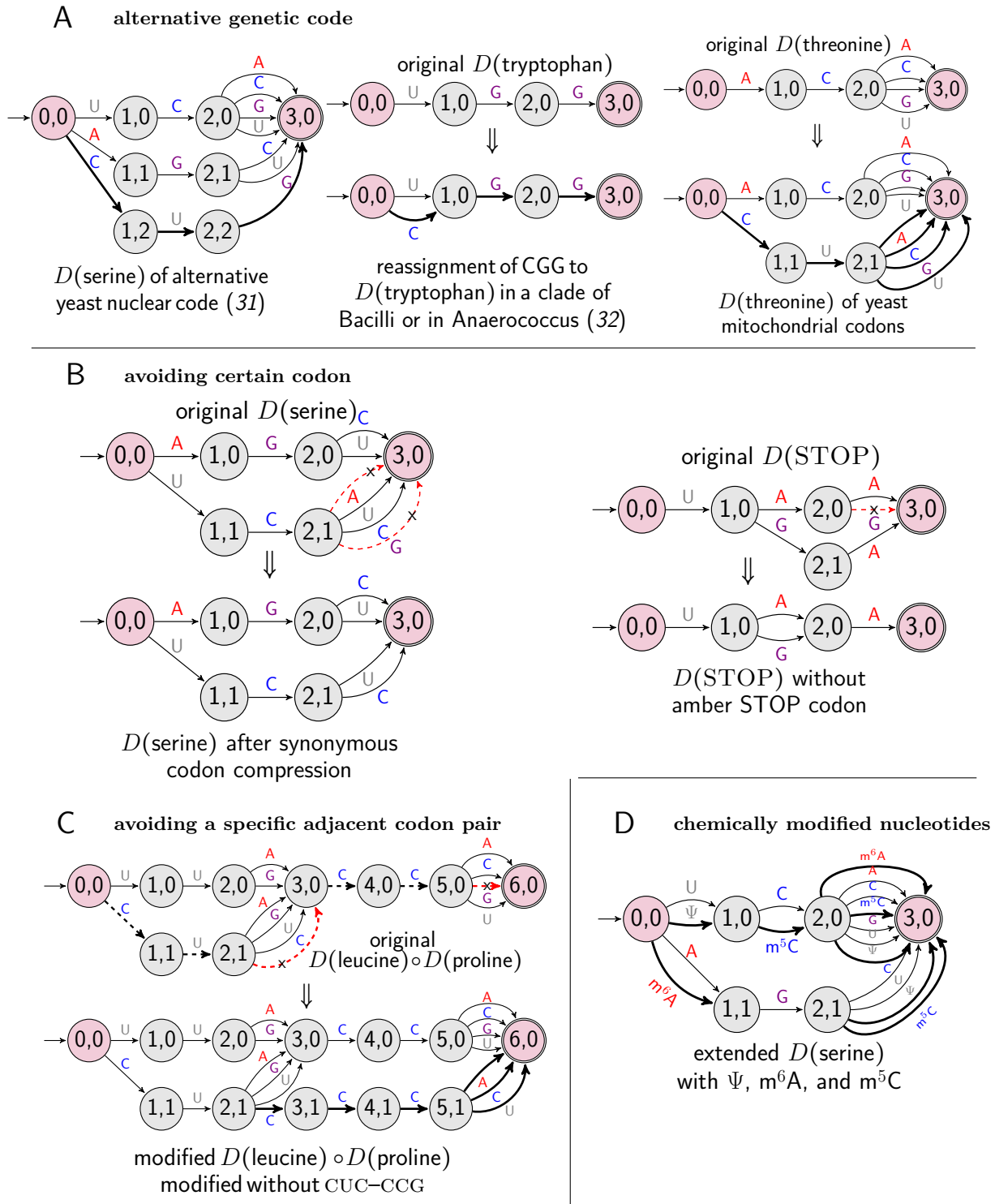


Figure S6: Examples of the DFA representations for extended codons, modified nucleotides, and coding constraints. **A**: Alternative genetic codes of serine, tryptophan, and threonine. **B**: Avoiding certain codon. On the left it shows the original DFA of serine (up), in which the red dashed arrows indicating UCA and UCG are chosen to be avoided, resulting in a new DFA (down) (33). On the right it shows removing the rare amber STOP codon (UAG) (33). **C**: Avoiding a specific adjacent codon pair. **D**: Extended serine DFA can include chemically modified nucleotides pseudouridine (Ψ), 6-Methyladenosine (m^6A) and 5-methylcytosine (m^5C).

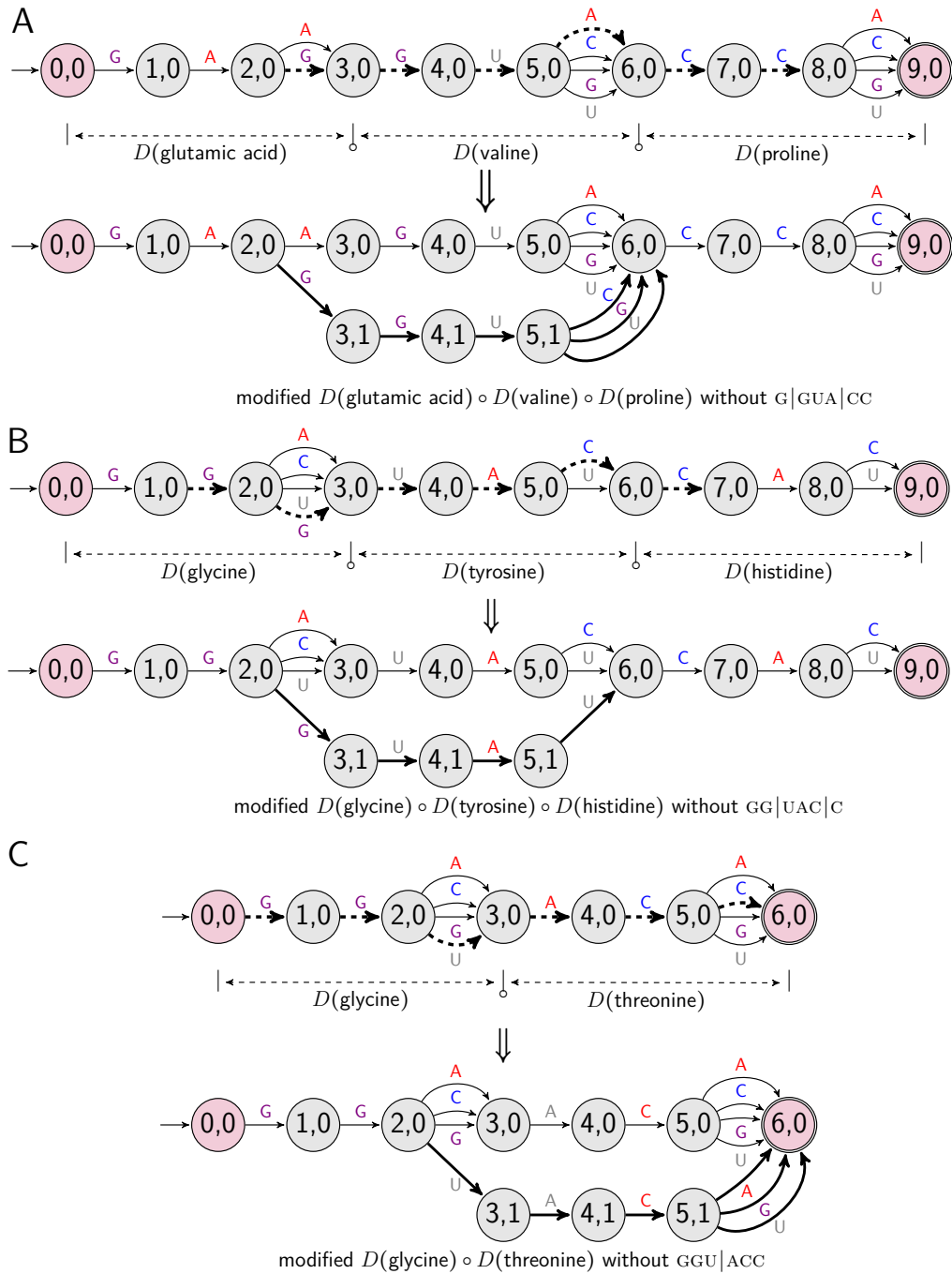


Figure S7: Avoiding a restriction enzyme specific recognition sequence (KpnI restriction enzyme recognition site: GGUACC). The enzyme recognition sequence is beyond one codon. **A–C** show three different partitions that split the sequence into different codons. See Fig. S6C for an example that avoids a specific adjacent codon pair.

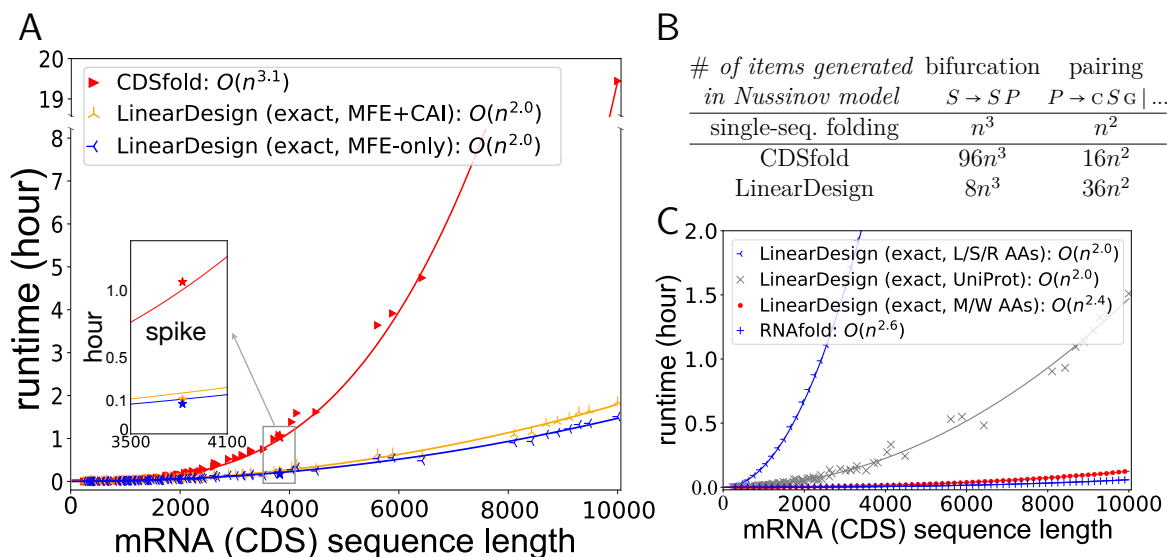


Figure S8: More *In silico* time complexity analysis. **A**: Runtime comparison between LinearDesign and CDSfold on UniProt proteins. Overall, LinearDesign is substantially faster than CDSfold, and more importantly, LinearDesign scales $O(n^2)$ empirically, where n is mRNA sequence length, while CDSfold runs in $O(n^{3.1})$; this difference can be explained by the analysis in **B**. On the other hand, our MFE+CAI mode (with $\lambda = 3$) is only slightly slower than our MFE-only version, while CDSfold cannot jointly optimize MFE and CAI. **B**: LinearDesign’s cubic-time bifurcation rule is so efficient that it is dominated by the quadratic-time pairing rule in practice. **C**: Runtime comparison of LinearDesign on proteins with most ambiguous (6-codon) amino acids, natural (UniProt) proteins, and proteins with unambiguous (1-codon) amino acids, the last of which is equivalent to single sequence folding. We also ran RNAfold on RNA sequences that encode the unambiguous amino acids. See also Fig. 3 for more *in silico* results of LinearDesign.

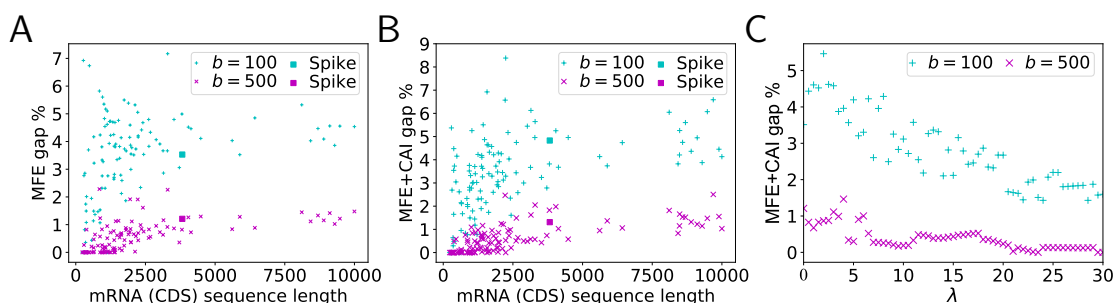


Figure S9: Search error of LinearDesign’s beam search mode against sequence length and λ (the weight of CAI in the joint optimization). **A–B**: Search error is relatively small, and does not deteriorate with sequence length. Here we used beam sizes 500 (purple) and 100 (cyan), on UniProt proteins (crosses) and SARS-CoV-2 Spike protein (squares), and we use $\lambda = 3$ for **B**. **C**: Search error decreases with λ . Note that the search error in **A** is the free energy gap % for $\lambda = 0$, defined as $1 - \text{MFE}(\mathbf{r}_{\text{approx_design}}) / \text{MFE}(\mathbf{r}_{\text{exact_design}})$; the search error in **B–C** is defined as $1 - \text{MFECAI}_\lambda(\mathbf{r}_{\text{approx_design}}) / \text{MFECAI}_\lambda(\mathbf{r}_{\text{exact_design}})$, where $\mathbf{r}_{\text{approx_design}}$ and $\mathbf{r}_{\text{exact_design}}$ are designed mRNAs from the beam search mode and the exact search mode, respectively. See also Fig. 3 for more *in silico* results.

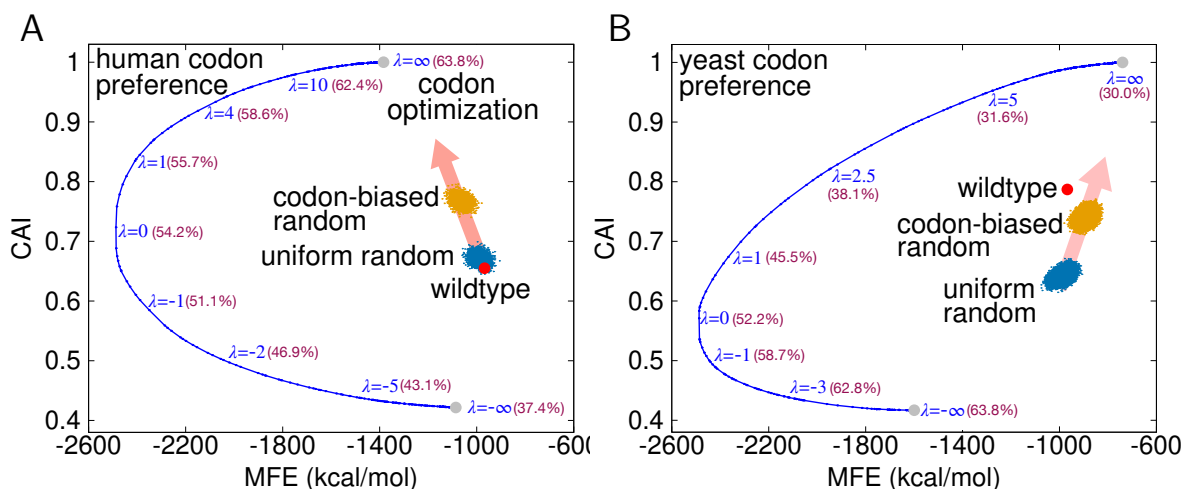


Figure S10: MFE-CAI two dimensional visualizations of Spike designs using human codon preference (A) and yeast codon preference (B) with positive and negative λ 's. GC% are shown in parentheses. The human genome prefers GC-rich codons that leads to higher CAI designs are with higher GC%, while the yeast genome prefers AU-rich codons that exhibits an opposite relationship between CAI and GC%. See also Fig. 3 for more *in silico* results of LinearDesign.

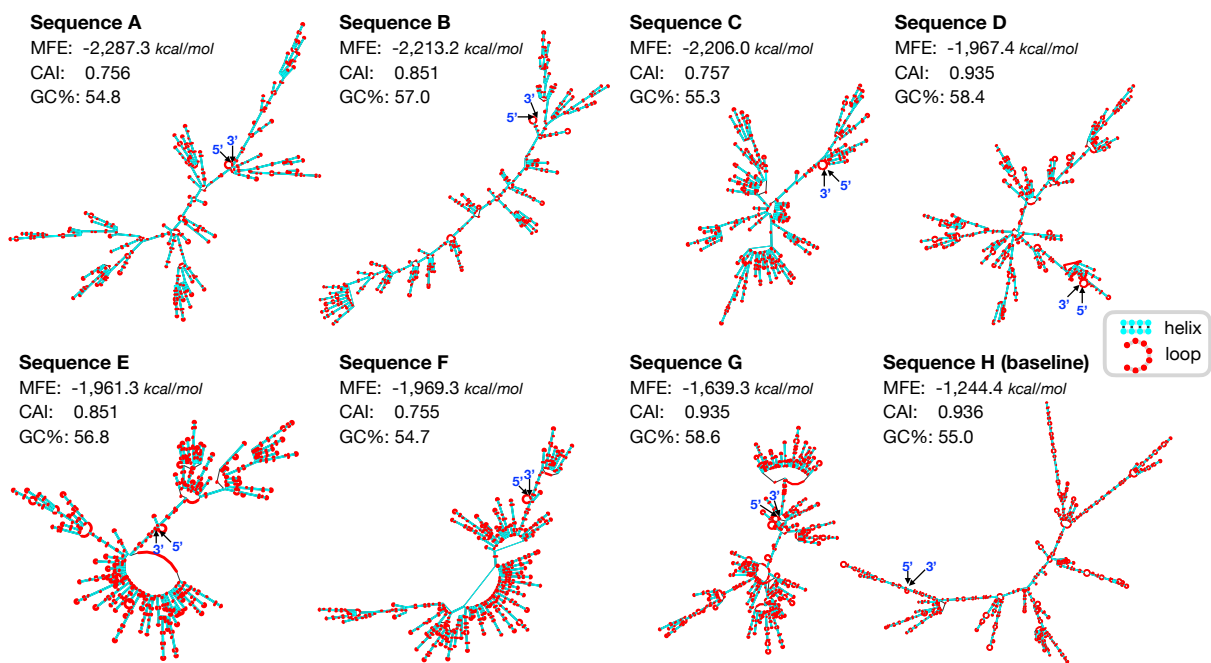


Figure S11: The secondary structures of LinearDesign-generated sequences (A-G) and the baseline sequence (H) used in the wet lab experiments. The stable helices are in cyan and unstable loops are in red. Sequences A-D clearly have less and smaller loops, and they have higher levels of antibody responses compared to the baseline H (see Fig. 4E-G). The secondary structures are predicted by Vienna RNAfold (-d0 mode) and visualized by RNAplot.

sequence of CDS	MFE			Molecular		
	(<i>kcal/mol</i>)	CAI	GC%	U%	weight	
A	-2,287.3	0.756	54.8	22.7	1,229,541	
B	-2,213.2	0.851	57.0	20.8	1,229,943	
C	-2,206.0	0.757	55.3	22.2	1,230,380	
D	-1,967.4	0.935	58.4	19.1	1,229,927	
E	-1,961.3	0.851	56.8	21.1	1,229,328	
F	-1,969.3	0.755	54.7	23.0	1,230,153	
G	-1,639.3	0.935	58.6	18.9	1,229,526	
H	-1,244.4	0.936	55.0	21.2	1,228,180	
MFE-Optimal	-2,486.7	0.732	54.3	22.9	1,229,980	
CAI-Optimal	-1,384.1	1.000	63.8	14.5	1,229,426	
Wildtype	-966.7	0.655	37.3	33.3	1,221,872	
CV2CoV	-1,384.4	0.903	63.9	15.7	1,226,373	
mRNA-1273	-1,369.2	0.978	62.3	15.5	1,229,366	
BNT-162b2	-1,217.2	0.946	57.0	19.1	1,227,844	

Table S1: Details of LinearDesign-generated sequences (A–G and MFE-Optimal), the baseline sequence (H), the CAI-optimal sequence, the wildtype sequence, and three vaccine sequences from CureVac, Moderna, and BioNTech. See Fig. 4 for more details of *in vitro* and *in vivo* experiment results. CDS sequences have no stop codon added.

sequence of CDS	MFE of CDS	Stemirna UTRs			BioNTech UTRs			Moderna UTRs			CureVac UTRs			human β -globin UTRs							
	<i>kcal/mol</i>	MFE	tot.	5' 3'	MFE	tot.	5' 3'	MFE	tot.	5' 3'	MFE	tot.	5' 3'	MFE	tot.	5' 3'					
A	-2287.3	-2325.1	14	12	2	-2378.0	8	5	3	-2333.3	12	10	2	-2313.4	5	5	0	-2327.2	9	0	9
B	-2213.2	-2252.1	15	13	2	-2302.0	5	5	0	-2258.1	14	12	2	-2235.7	5	5	0	-2252.0	29	0	29
C	-2206.0	-2240.8	10	8	2	-2294.1	6	6	0	-2248.1	10	8	2	-2229.7	17	17	0	-2242.3	11	7	4
D	-1967.4	-2002.5	13	9	4	-2056.4	10	5	5	-2010.7	12	10	2	-1991.8	3	0	3	-2005.8	14	0	14
E	-1961.3	-1999.1	14	12	2	-2057.3	15	5	10	-2008.9	16	14	2	-1989.6	19	12	7	-2002.2	18	0	18
F	-1969.3	-2006.5	11	9	2	-2060.9	11	5	6	-2014.2	6	0	6	-1993.8	11	0	11	-2007.4	9	0	9
G	-1639.3	-1681.5	23	5	18	-1743.0	33	4	29	-1686.8	61	0	61	-1673.4	22	22	0	-1687.3	46	11	35
H	-1244.4	-1284.9	18	8	10	-1345.3	72	8	64	-1292.9	25	17	8	-1285.5	27	19	8	-1291.4	21	0	21
CureVac	-1384.4	-1424.4	21	5	16	-1479.0	33	5	28	-1430.5	82	26	56	-1419.4	76	61	15	-1425.5	20	0	20
Moderna	-1369.2	-1411.6	29	4	25	-1464.3	24	4	20	-1419.1	59	12	47	-1406.6	63	45	18	-1418.3	26	0	26
BioNTech	-1217.2	-1259.1	34	5	29	-1316.3	98	6	92	-1266.3	47	15	32	-1253.9	58	54	4	-1265.6	42	6	36
MFE-opt.	-2486.7	-2522.3	3	3	0	-2575.9	1	1	0	-2532.2	3	3	0	-2512.5	2	2	0	-2522.6	13	0	13
CAI-opt.	-1384.1	-1424.1	29	4	25	-1478.0	58	0	58	-1430.9	35	7	28	-1420.4	53	53	0	-1431.5	33	5	28
Wildtype	-966.7	-1007.0	21	19	2	-1060.6	29	21	8	-1019.1	27	25	2	-1000.3	18	18	0	-1011.7	56	9	47

Table S2: The numbers of base pairs formed between UTRs and the mRNA coding region, i.e., one base of the pairs is in 5' or 3'-UTR, and the other is in the coding region. Here we used 5 different UTRs: Stemirna UTRs used in wet lab experiments, BNT-162b2 (BioNTech) UTRs, mRNA-1273 (Moderna) UTRs, CV2CoV (CureVac) UTRs, and a widely-used human β -globin mRNA UTRs. We tested 14 different sequences of the coding region: sequences A–H in for wet lab experiments, sequences from three main mRNA vaccine companies, MFE-opt. and CAI-opt. sequences (i.e., sequences with the lowest folding free energy and with CAI=1, respectively), and the wildtype sequence. Most of the LinearDesign-generated mRNA sequences (sequences A–F and MFE-opt., shaded in light cyan) form fewer base pairs with UTRs. The folding free energies and structures are predicted by Vienna RNAfold (-d0 mode); MFEs of CDS are calculated without stop codon.

References In Supplementary Materials

1. Sharp PM, Li WH (1987) The codon adaptation index—a measure of directional synonymous codon usage bias, and its potential applications. *Nucleic Acids Research* 15(3):1281–1295.
2. Rivas E (2013) The four ingredients of single-sequence RNA secondary structure prediction. a unifying perspective. *RNA Biology* 10(7):1185–1196.
3. Nussinov R, Jacobson AB (1980) Fast algorithm for predicting the secondary structure of single-stranded RNA. *Proceedings of the National Academy of Sciences U.S.A.* 77(11):6309–6313.
4. Kasami T (1966) An efficient recognition and syntax-analysis algorithm for context-free languages. *Coordinated Science Laboratory Report no. R-257*.
5. Younger DH (1967) Recognition and parsing of context-free languages in time n^3 . *Information and Control* 10(2):189–208.
6. Rivas E, Lang R, Eddy. R (2012) A range of complex probabilistic models for RNA secondary structure prediction that includes the nearest-neighbor model and more. *RNA* 18(2):193–212.
7. Bar-Hillel Y, Perles M, Shamir E (1961) On formal properties of simple phrase structure grammars. *Zeitschrift für Phonetik, Sprachwissenschaft und Kommunikationsforschung* 14(2):143–172.
8. Huang L, et al. (2019) LinearFold: linear-time approximate RNA folding by 5'-to-3' dynamic programming and beam search. *Bioinformatics* 35(14):i295–i304.
9. Huang L, Fayong S, Guo Y (2012) Structured perceptron with inexact search in *Proceedings of the 2012 Conference of the North American Chapter of the Association for Computational Linguistics: Human Language Technologies*. (Association for Computational Linguistics, Montréal, Canada), pp. 142–151.
10. Mathews DH, Sabina J, Zuker M, Turner DH (1999) Expanded sequence dependence of thermodynamic parameters improves prediction of RNA secondary structure. *Journal of Molecular Biology* 288(5):911–940.

11. Mathews DH, et al. (2004) Incorporating chemical modification constraints into a dynamic programming algorithm for prediction of RNA secondary structure. *Proceedings of the National Academy of Sciences U.S.A.* 101(19):7287–7292.
12. Lorenz R, et al. (2011) ViennaRNA package 2.0. *Algorithms for Molecular Biology* 6(1):1.
13. Turner DH, Mathews DH (2010) NNDB: the nearest neighbor parameter database for predicting stability of nucleic acid secondary structure. *Nucleic Acids Research* 38(suppl_1):D280–D282.
14. Kawaguchi Y, Honda H, Taniguchi-Morimura J, Iwasaki S (1989) The codon CUG is read as serine in an asporogenic yeast *Candida cylindracea*. *Nature* 341(6238):164–166.
15. Bonitz SG, et al. (1980) Codon recognition rules in yeast mitochondria. *Proceedings of the National Academy of Sciences U.S.A.* 77(6):3167–3170.
16. Gamble CE, Brule CE, Dean KM, Fields S, Grayhack EJ (2016) Adjacent codons act in concert to modulate translation efficiency in yeast. *Cell* 166(3):679–690.
17. Karikó K, et al. (2008) Incorporation of pseudouridine into mRNA yields superior nonimmunogenic vector with increased translational capacity and biological stability. *Molecular Therapy* 16(11):1833–1840.
18. Cohen B, Skiena S (2003) Natural selection and algorithmic design of mRNA. *Journal of Computational Biology* 10(3-4):419–432.
19. Terai G, Kamegai S, Asai K (2016) CDSfold: an algorithm for designing a protein-coding sequence with the most stable secondary structure. *Bioinformatics* 32(6):828–834.
20. Mauger DM, et al. (2019) mRNA structure regulates protein expression through changes in functional half-life. *Proceedings of the National Academy of Sciences U.S.A.* 116(48):24075–24083.
21. Consortium U (2005) UniProt: a hub for protein information. *Nucleic Acids Research* 42:D204–D12.

22. Ding Y, et al. (2013) In vivo genome-wide profiling of RNA secondary structure reveals novel regulatory features. *Nature* 505.
23. Wan Y, et al. (2014) Landscape and variation of RNA secondary structure across the human transcriptome. *Nature* 505:706–709.
24. Shah P, Ding Y, Niemczyk M, Kudla G, Plotkin JB (2013) Rate-limiting steps in yeast protein translation. *Cell* 153:1589–601.
25. Tuller T, Zur H (2014) Multiple roles of the coding sequence 5' end in gene expression regulation. *Nucleic Acids Research* 43(1):13–28.
26. Liu L, et al. (2008) Structural basis of toll-like receptor 3 signaling with double-stranded RNA. *Science* 320(5874):379–381.
27. Husain B, Mukerji I, Cole JL (2012) Analysis of high-affinity binding of protein kinase R to double-stranded RNA. *Biochemistry* 51(44):8764–8770.
28. Hur S (2019) Double-stranded RNA sensors and modulators in innate immunity. *Annual Review of Immunology* 37:349–375.
29. Persano S, et al. (2017) Lipopolyplex potentiates anti-tumor immunity of mRNA-based vaccination. *Biomaterials* 125:81–89.
30. Tan CW, et al. (2020) A SARS-CoV-2 surrogate virus neutralization test based on antibody-mediated blockage of ACE2–spike protein–protein interaction. *Nature Biotechnology* 38(9):1073–1078.
31. Ohama T, et al. (1993) Non-universal decoding of the leucine codon CUG in several *Candida* species. *Nucleic Acids Research* 21(17):4039–4045.
32. Shulgina Y, Eddy SR (2021) A computational screen for alternative genetic codes in over 250,000 genomes. *eLife* 10:e71402.
33. Fredens J, et al. (2019) Total synthesis of *Escherichia coli* with a recoded genome. *Nature* 569(7757):514–518.